Elongation factor ELOF1 drives transcription-coupled repair and prevents genome instability

Geijer, Marit E; Zhou, Di; Selvam, Kathiresan; Steurer, Barbara; Mukherjee, Chirantani; Evers, Bastiaan; Cugusi, Simona; van Toorn, Marvin; van der Woude, Melanie; Janssens, Roel C

Published in:
Nature Cell Biology

DOI:
10.1038/s41556-021-00692-z

Publication date:
2021

ARTICLES
https://doi.org/10.1038/s41556-021-00692-z

nature cell biology

Elongation factor ELOF1 drives transcription-coupled repair and prevents genome instability

Marit E. Geijer[1], Di Zhou[1,11], Kathiresan Selvam[2,11], Barbara Steurer[1,11], Chirantani Mukherjee[1,11], Bastiaan Evers[3,11], Simona Cugusi[4,11], Marvin van Toorn[1], Melanie van der Woude[1], Roel C. Janssens[1], Yannick P. Kok[5], Wenzhi Gong[6], Anja Raams[1], Calvin S. Y. Lo[1], Joyce H. G. Lebbink[1,7], Bart Geverts[8], Dalton A. Plummer[2], Karel Bezstarosti[9], Arjan F. Theil[1], Richard Mitter[10], Adriaan B. Houtsmuller[8], Wim Vermeulen[1], Jeroen A. A. Demmers[9], Shisheng Li[6], Marcel A. T. M. van Vugt[5], Hannes Lans[1], René Bernards[3], Jesper Q. Svejstrup[4], Arnab Ray Chaudhuri[1], John J. Wyrick[2] and Jurgen A. Marteijn[1]✉

Correct transcription is crucial for life. However, DNA damage severely impedes elongating RNA polymerase II, causing transcription inhibition and transcription-replication conflicts. Cells are equipped with intricate mechanisms to counteract the severe consequence of these transcription-blocking lesions. However, the exact mechanism and factors involved remain largely unknown. Here, using a genome-wide CRISPR–Cas9 screen, we identified the elongation factor ELOF1 as an important factor in the transcription stress response following DNA damage. We show that ELOF1 has an evolutionarily conserved role in transcription-coupled nucleotide excision repair (TC-NER), where it promotes recruitment of the TC-NER factors UVSSA and TFIIH to efficiently repair transcription-blocking lesions and resume transcription. Additionally, ELOF1 modulates transcription to protect cells against transcription-mediated replication stress, thereby preserving genome stability. Thus, ELOF1 protects the transcription machinery from DNA damage via two distinct mechanisms.

Faithful transcription is essential for proper cell function. However, transcription is continuously threatened by DNA-damaging agents, which induce transcription-blocking lesions (TBLs) that strongly impede or completely block the progression of RNA polymerase II (Pol II). Impeded transcription elongation by DNA damage can affect transcription fidelity or result in a complete absence of newly synthesized mRNA transcripts. This can lead to severe cellular dysfunction, senescence and cell death, consequently contributing to ageing[1]. Furthermore, prolonged stalling of Pol II at TBLs can form an obstacle for the replication machinery, thereby giving rise to transcription-replication conflicts. These conflicts can lead to genome instability and the onset of cancer[2,3]. Cells are equipped with an intricately regulated cellular response to overcome these severe consequences of TBLs. This transcription stress response includes repair of TBLs and mechanisms to overcome transcription-replication conflicts[1,2].

The main mechanism to remove TBLs is transcription-coupled nucleotide excision repair (TC-NER). TC-NER removes a wide spectrum of environmentally or endogenously induced TBLs, including ultraviolet (UV)-light-induced lesions and oxidative damage[1]. The biological relevance of TC-NER is best illustrated by Cockayne syndrome (CS), which is characterized by photosensitivity, progressive neurodegeneration and premature ageing[4], and is caused by inactivating mutations in TC-NER genes. The TC-NER initiating factor CSB (also known as ERCC6) is recruited after Pol II stalling. CSB uses its forward translocating ability to discriminate between lesion-stalled and other forms of paused Pol II[5]. When lesion-stalled Pol II is recognized, the full TC-NER complex is assembled by the recruitment of CSA (also known as ERCC8), which is part of a cullin 4–RING E3 ubiquitin ligase complex ($CRL4^{CSA}$)[6], and UVSSA[7]. Recently, it was shown that the ubiquitylation of lesion-stalled Pol II plays an important role in TC-NER complex assembly and in the transcription stress response[8,9]. UVSSA subsequently promotes the recruitment of TFIIH[7,10], which forms the core incision complex with XPA and RPA. This complex recruits the endonucleases XPG and ERCC1–XPF to excise the TBL[11]. Repair is finalized by refilling and ligating the gap, after which transcription can restart[1].

Although several key factors have been identified in the cellular response to DNA-damage-induced transcription stress, the exact molecular mechanism of how cells repair TBLs and avoid collisions of lesion-stalled Pol II with the replication machinery remain largely unknown.

[1]Department of Molecular Genetics, Oncode Institute, Erasmus MC Cancer Institute, Erasmus University Medical Center, Rotterdam, The Netherlands. [2]School of Molecular Biosciences, Washington State University, Pullman, WA, USA. [3]Oncode Institute, Division of Molecular Carcinogenesis, The Netherlands Cancer Institute, Amsterdam, The Netherlands. [4]Mechanisms of Transcription Laboratory, The Francis Crick Institute, London, UK. [5]Department of Medical Oncology, University Medical Center Groningen, University of Groningen, Groningen, The Netherlands. [6]Department of Comparative Biomedical Sciences, School of Veterinary Medicine, Louisiana State University, Baton Rouge, LA, USA. [7]Department of Radiation Oncology, Erasmus University Medical Center, Rotterdam, The Netherlands. [8]Erasmus Optical Imaging Center, Erasmus University Medical Center Rotterdam, Rotterdam, The Netherlands. [9]Proteomics Center, Erasmus University Medical Center, Rotterdam, The Netherlands. [10]Bioinformatics and Biostatistics, The Francis Crick Institute, London, UK. [11]These authors contributed equally: Di Zhou, Kathiresan Selvam, Barbara Steurer, Chirantani Mukherjee, Bastiaan Evers, Simona Cugusi. ✉e-mail: J.Marteijn@erasmusmc.nl

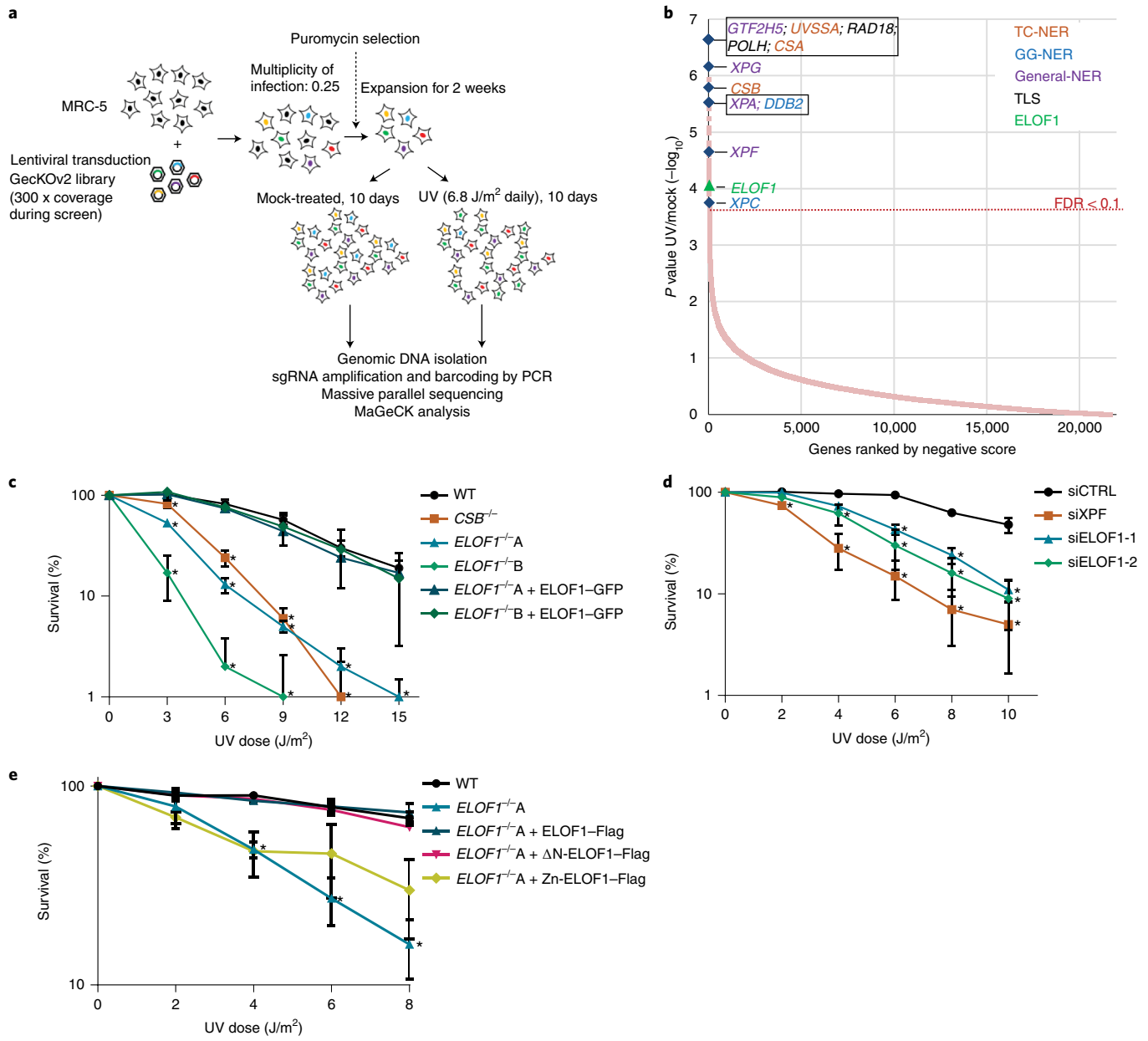

Fig. 1 | Genome-wide CRISPR–Cas9 screen identifies ELOF1 as a factor involved in the UV-induced DNA-damage response. a, Schematic of the CRISPR–Cas9 screen. MRC-5 (SV40) cells were transduced with a lentiviral sgRNA library[12]. The resulting pool of gene-edited cells was split into a control and a UV-irradiated group. Cells were respectively mock-treated or daily UV-irradiated with 6.8 J/m² UV for ten consecutive days, thereby maintaining ~50% cell confluency throughout the screen (Extended Data Fig. 1a). sgRNA abundance was determined by next-generation sequencing of PCR-amplified incorporated sgRNAs from the isolated genomic DNA of surviving cell pools[48]. UV-sensitive genes were identified by comparing the abundance in UV-irradiated cells over mock-treated cells using MAGecK analysis. The screen was performed in duplicate. **b**, UV-sensitive genes were ranked based on the gene-based *P* value resulting from MaGeCK analysis of the change in abundance of sgRNAs in UV-treated over mock-treated. Genes involved in NER or TLS are colour-coded. **c**, Relative colony survival of HCT116 WT cells, indicated KO cells (−/−) or rescued cells exposed to the indicated doses of UV. **d**, Relative colony survival of MRC-5 cells transfected with the indicated siRNAs following exposure to the indicated doses of UV. **e**, Relative colony survival of HCT116 *ELOF1* KO cells with expression of the indicated ELOF1 mutants following exposure to the indicated doses of UV. ΔN, deletion of the N terminus; Zn, zinc-finger mutant. Data shown in **c**–**e** represent the mean ± s.e.m. ($n = 3$ independent experiments) $^*P \leq 0.05$ relative to WT/siCTRL analysed by one-sided unpaired *t*-test. Numerical data are provided in the source data.

Results

ELOF1 protects against UV-induced DNA damage. To identify factors involved in the DNA-damage-induced transcription stress response, we performed a genome-wide CRISPR–Cas9 loss-of-function screen following UV-induced DNA damage. Briefly, fibroblasts were transduced with a lentiviral single guide RNA (sgRNA) library[12] and UV-irradiated for ten consecutive days (Fig. 1a and Extended Data Fig. 1a). sgRNA abundance was determined by next-generation sequencing and was compared with untreated cells using model-based analysis of genome-wide CRISPR–Cas9 knockout (MAGeCK) analysis[13] (Fig. 1b and Supplementary Table 1). Gene ontology (GO) analysis of the top UV-sensitive hits (false-discovery rate (FDR) < 0.1) identified many genes involved in the UV-induced DNA-damage response (Extended Data

Fig. 1b), such as translesion synthesis (TLS) factors[14], and many NER genes[11]. In particular, the identification of the key TC-NER factors *CSA*, *CSB* and *UVSSA* underscored the potential of this screen to identify factors involved in the DNA-damage-induced transcription stress response.

One of the top UV-sensitive hits was elongation factor 1 homologue (*ELOF1*), an evolutionarily conserved small zinc-finger protein (~10 kDa)[15]. Its orthologue, *ELF1*, was identified in budding yeast, whereby *ELF1* disruption was synthetically lethal with mutations in genes encoding elongation factors such as *SPT6* and *TFIIS*[16]. Follow-up studies using yeast revealed that Elf1 interacts with the elongation complex[16–19], and in vitro studies showed that Elf1 binds downstream of Pol II at the DNA entry tunnel and promotes elongation through nucleosomes[20]. However, its exact function and its role in the DNA-damage response thus far remains unknown.

To validate the UV sensitivity of cells after ELOF1 depletion, we performed clonogenic survival experiments using two independent *ELOF1* knockout (KO) HCT116 cell lines (Extended Data Fig. 1c–g). ELOF1 deficiency resulted in severe UV hypersensitivity that was to the same level as in TC-NER-deficient *CSB* KO cells (Fig. 1c). Similar results were obtained after short interfering RNA (siRNA)-mediated ELOF1 depletion (Fig. 1d and Extended Data Fig. 1h,i). ELOF1 re-expression in *ELOF1* KO cells fully rescued UV sensitivity, which indicates that the observed effects are specific for ELOF1. Although the amino-terminal tail of ELOF1 promotes Pol II progression on the nucleosome[20], absence of this tail could still rescue the UV sensitivity effect (Fig. 1f and Extended Data Fig. 1j). However, the conserved zinc-finger domain of ELOF1 was crucial for UV survival. Furthermore, photolyase-mediated reversal[21] of UV-induced cyclobutane pyrimidine dimers (CPDs) almost completely rescued the UV sensitivity of *ELOF1* KO cells, which shows that this sensitivity is due to DNA damage and not RNA or protein damage (Extended Data Fig. 1k).

ELOF1 is a transcription elongation factor. We first tested whether ELOF1 is part of the elongating Pol II complex, as previously observed in yeast[16–20]. We generated homozygous *ELOF1–mScarletI–HA* knock-in (KI) cells to detect endogenously expressed ELOF1 (Extended Data Fig. 2a). ELOF1 was localized strictly to the nucleus, excluded from the nucleoli and showed high levels of colocalization with Pol II (Fig. 2a and Extended Data Fig. 2b,c). Live-cell imaging studies of green fluorescent protein (GFP)–RPB1 mobility showed that fluorescence recovery after photobleaching (FRAP) experiments are a sensitive way to study Pol-II-mediated transcription[22]. Therefore, we compared the mobility of ELOF1 to that of Pol II and observed that it was almost identical to the level in non-treated conditions (Fig. 2b). The large degree of ELOF1 immobilization suggests that the majority of ELOF1 molecules are chromatin bound, most probably engaged in transcription elongation, similar to that observed for Pol II[22]. The engagement of ELOF1 in transcription elongation was confirmed by its swift chromatin release, as shown by its strong mobilization after transcription inhibition (Fig. 2b). This almost complete mobilization effect suggests that ELOF1 is exclusively involved in transcription-related processes.

To further investigate whether ELOF1 is part of the elongating Pol II complex, we performed immunoprecipitation (IP) experiments and showed that ELOF1 interacts with RPB1 and RPB3, both of which are subunits of Pol II (Fig. 2c). The interaction of ELOF1 with P-Ser2-modified RPB1, which primarily marks elongating Pol II, indicates that ELOF1 is present in the elongation complex, which was confirmed by the reciprocal IP experiment (Extended Data Fig. 2d). Moreover, stable isotope labelling of amino acids in culture (SILAC)-based interaction proteomics of endogenously expressed GFP–RPB1 (ref. [22]) identified ELOF1 as a Pol II interactor, with similar SILAC ratios to that of other elongation factors (Extended Data Fig. 2e and Supplementary Table 2). To obtain a complete overview of ELOF1-interacting proteins, we performed SILAC-based interaction proteomics for ELOF1, and this revealed high SILAC ratios for many Pol II subunits and elongation factors, including TFIIS, SPT5, SPT6 and the PAF complex (Fig. 2d and Supplementary Table 2). GO analysis of the ELOF1 interactors revealed its involvement in transcription-related processes (Extended Data Fig. 2f). Of note, the ELOF1–Pol II interaction did not change after UV-induced DNA damage, which is in contrast to the Pol II–CSB interaction[23] (Fig. 2c and Extended Data Fig. 2d). These data indicate that ELOF1 is an integral component of the transcription elongation complex, independent of DNA damage.

Next, we tested whether ELOF1 acts as a transcription elongation factor by determining its effect on Pol II elongation rates using DRB/TT$_{chem}$-seq[24]. Nascent RNA was labelled with 4SU to determine the Pol II position in gene bodies at different time points after its release from the promoter by DRB washout (Fig. 2e). Single-gene profiles (Extended Data Fig. 3a) and metagene analysis of >200 kb genes (Fig. 2e,f) showed that *ELOF1* KO resulted in a clear decreased average elongation rate from 2.6 kb min^{-1} to 2.0 kb min^{-1}, while an approximately sixfold overexpression of ELOF1 (Extended Data Fig. 1f) resulted in an increased average elongation rate to 3.1 kb min^{-1}. In contrast, loss of CSB had no obvious effect on the Pol II elongation rate. Comparable results were obtained for shorter genes (Extended Data Fig. 3a,b). In line with this reduced elongation rate, the overall nascent RNA synthesis level was also reduced after ELOF1 depletion (Extended Data Fig. 3c–e).

To obtain mechanistic insights into the reduced elongation speed in *ELOF1* KO cells, we studied the differences in the P-Ser2-modified

Fig. 2 | ELOF1 is part of the elongating Pol II complex. a, Colocalization of endogenously expressed ELOF1 and Pol II in HCT116 cells with *ELOF1–mScarletI–HA* and *GFP–RPB1* KI cells during live-cell imaging. Scale bar, 10 µm. The experiment was performed two times, with similar results obtained. **b**, FRAP analysis of endogenously expressed ELOF1–mScarletI (left) and GFP–RPB1 (right). Cells were mock-treated (NT) or inhibited at different steps of the transcription cycle using the indicated inhibitors. Pol II initiation was inhibited with the CDK7 inhibitor THZ1 (ref. [49]) or promoter-pause release was inhibited by the CDK9 inhibitor flavopiridol[50]. The relative fluorescence intensity (RFI) was measured over time, background-corrected and normalized to the pre-bleach fluorescence intensity. *ELOF1* KI: NT $n=40$, THZ1 $n=24$, flavopiridol $n=24$ cells. *RPB1* KI: NT $n=21$, THZ1 $n=16$, flavopiridol $n=18$ cells. Data from three independent experiments. **c**, IP of ELOF1 using RFP beads in *ELOF1* KI cells followed by immunoblotting for the indicated proteins. Cells were collected 1 h after mock-treatment or irradiation with 16 J/m^2 UV. BC, binding control. The experiment was performed two times, with similar results obtained. **d**, Interaction heatmap of the SILAC ratios of ELOF1-interacting proteins as determined by quantitative interaction proteomics following HA IP of ELOF1. Average SILAC ratios of duplicate experiments are plotted and represent ELOF1 interactors relative to empty beads. A SILAC ratio >1 indicates an increase in interaction. Asterisk indicates proteins quantified in one experiment. **e**, Top: schematic of DRB/TT$_{chem}$-seq to measure Pol II elongation rates. Bottom: metagene profiles of >200 kb genes of DRB/TT$_{chem}$-seq in HCT116 WT or indicated KO cells, with ELOF1 re-expression where indicated, 10, 20, 30 or 40 min after DRB release. RPKM, reads per kilobase of transcript, per million mapped reads. **f**, Average elongation rates as determined by DRB/TT$_{chem}$-seq for >200 kb genes. **g**, Interaction heatmap based on the SILAC ratios as determined by quantitative interaction proteomics of P-Ser2-modified Pol II-interacting proteins in *ELOF1*$^{-/-}$A cells relative to WT cells. Average SILAC ratios of duplicate experiments are plotted. Asterisk indicates proteins quantified in one experiment. SILAC ratios <1 indicate loss of interaction, >1 indicate increase in interaction. Numerical data and uncropped blots are provided in the source data.

Pol II interactome with and without ELOF1 using SILAC-based proteomics. Absence of ELOF1 did not affect the presence of the core Pol II subunits or the majority of elongation factors (Fig. 2g and Supplementary Table 2). Interestingly, the biggest change in complex composition was found for CSA and CSB, with each having a fourfold increased Pol II interaction without ELOF1. Increased CSB binding might indicate that Pol II forward translocation is more frequently perturbed without ELOF1, since CSB recognizes stalled Pol II at DNA lesions and natural pause sites[5]. Such perturbation can stimulate Pol II backtracking and recruitment of TFIIS to stimulate transcript cleavage and transcription resumption[25]. In line with this, we observed an increased level of TFIIS binding to elongating Pol II in *ELOF1* KO cells (Fig. 2g). Furthermore, depletion of TFIIS gave rise to synthetic lethality with *ELOF1* KO cells (Extended Data Fig. 3f), as was also observed in yeast[16].

ELOF1 is essential for TC-NER. After having established that ELOF1 is a bona fide elongation factor, we studied its role in the

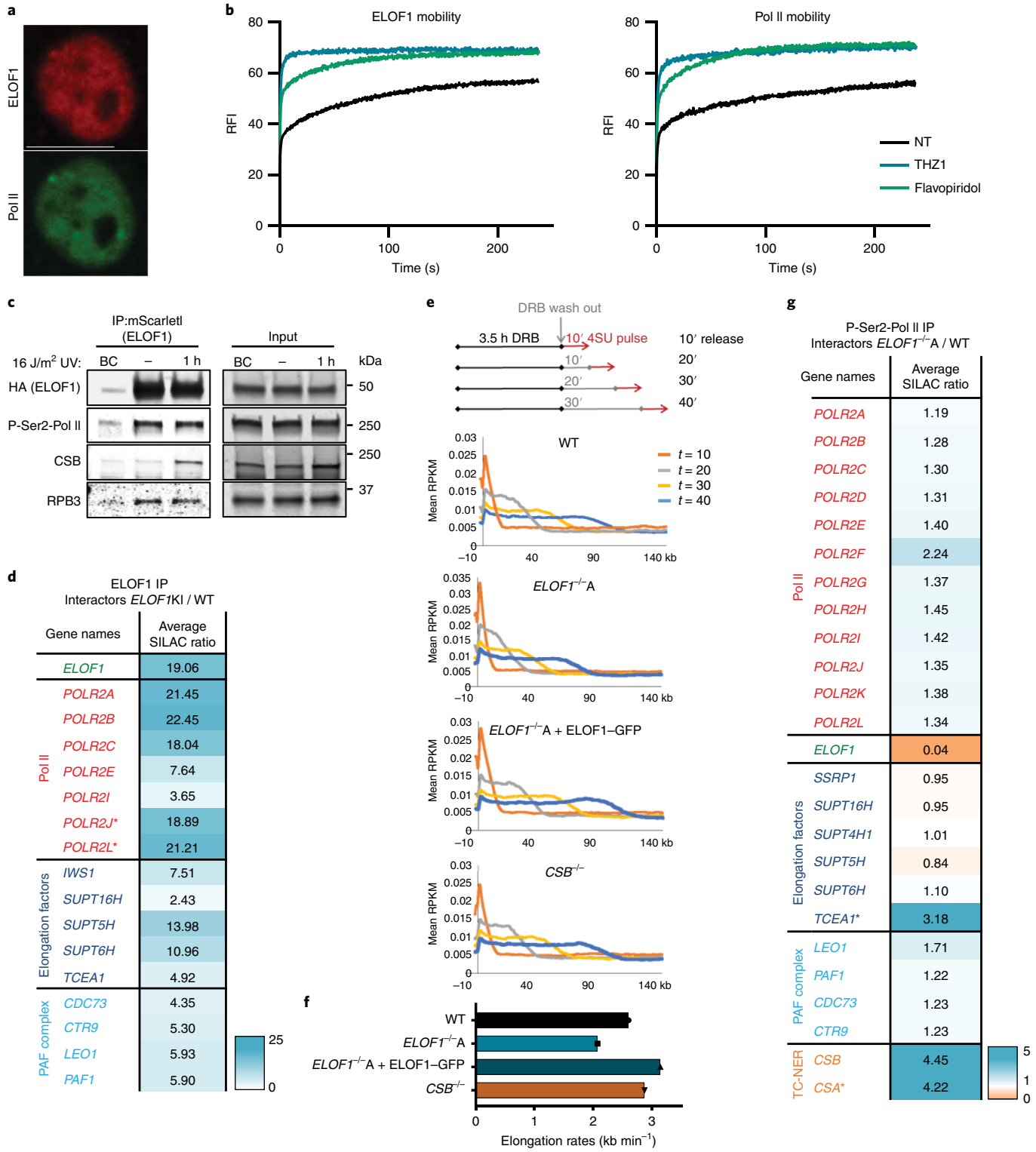

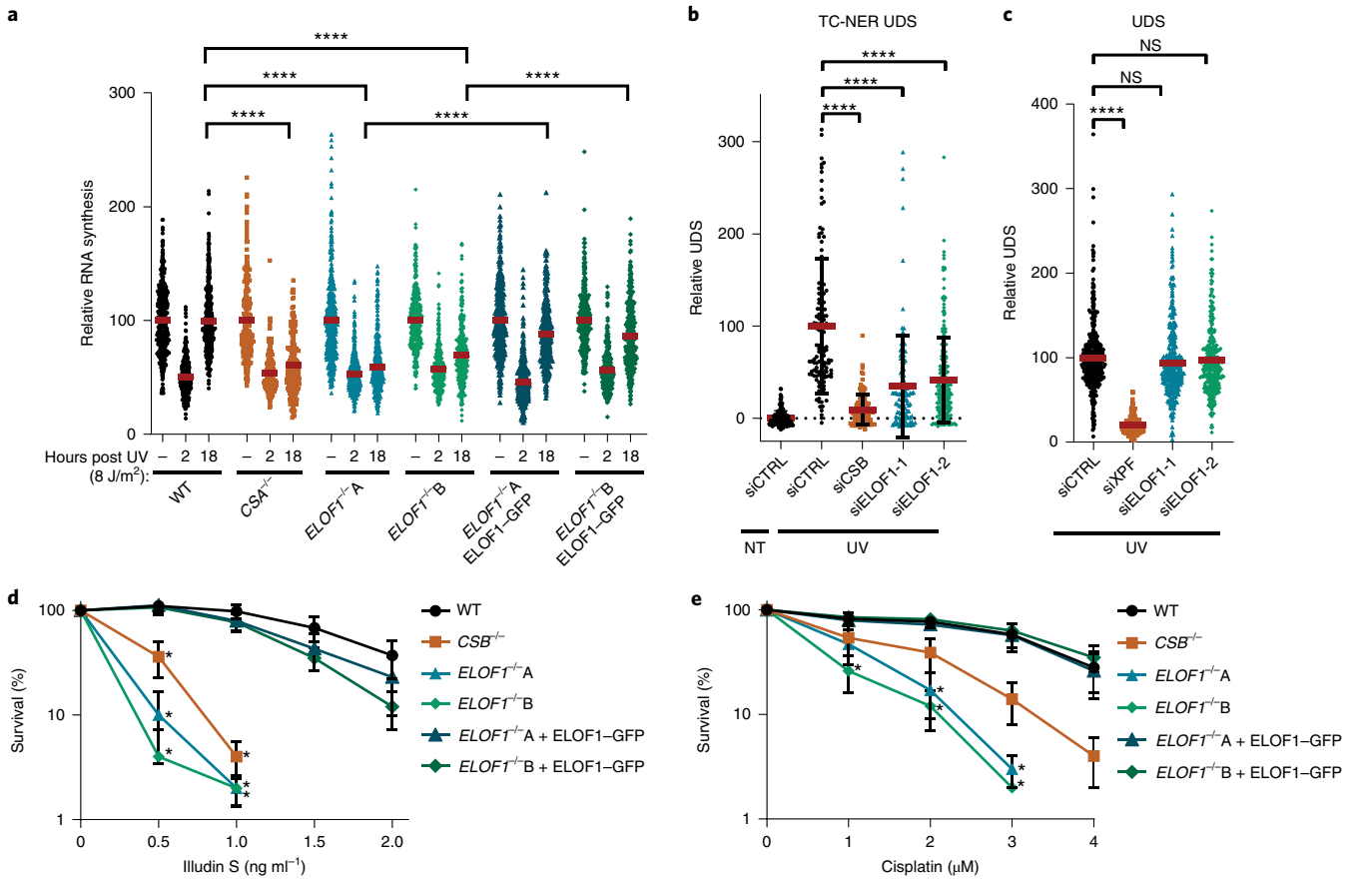

Fig. 3 | ELOF1 is important for functional TC-NER. a, Transcription restart after UV damage as determined by relative EU incorporation in the indicated HCT116 WT and KO cells, with ELOF1 re-expression where indicated, at the indicated time points after UV exposure (8 J/m²). The relative integrated density was normalized to mock-treated levels and set to 100%. Red lines indicate average integrated density ± s.e.m. from three independent experiments of (left to right) $n = 537, 528, 496, 227, 222, 203, 455, 421, 431, 458, 450, 405, 499, 495, 406, 470, 432$ and 446 cells. **b**, TC-NER-specific UDS as determined by relative EdU incorporation (for 7 h) in XP186LV fibroblasts (XP-C) transfected with the indicated siRNAs following UV-irradiation (8 J/m²). Cells from two independent experiments were analysed. NT: siCTRL $n = 193$; UV: siCTRL $n = 127$, siCSB $n = 132$, siELOF1-1 $n = 108$, siELOF1-2 $n = 217$. **c**, Relative levels of EdU incorporation (for 3 h) in C5RO (hTert) cells transfected with the indicated siRNAs following UV-irradiation (16 J/m²). Cells from three independent experiments were analysed. siCTRL $n = 356$, siXPF $n = 203$, siELOF1-1 $n = 363$, siELOF1-2 $n = 348$. **d**,**e**, Relative colony survival of the indicated HCT116 WT and KO cells, with ELOF1 re-expression where indicated, after a 24-h exposure to the indicated concentrations of illudin S (**d**) or cisplatin (**e**). Illudin S: mean ± s.e.m. $n = 3$ independent experiments for all conditions except *ELOF1*$^{-/-}$B: $n = 2$ independent experiments. Cisplatin: $n = 4$ independent experiments. $^{*}P \leq 0.05$, $^{****}P \leq 0.0001$, NS, not significant; two-sided unpaired *t*-test (**a**–**c**) or one-sided unpaired *t*-test (**d**,**e**). Numerical data are provided in the source data.

DNA-damage response. Since *ELOF1* KO cells are sensitive to UV-induced DNA damage, which is a potent inhibitor of transcription, we tested whether ELOF1 is needed for recovery of transcription after UV exposure by quantifying nascent transcription levels by 5-ethynyl uridine (EU) incorporation[26]. Transcription was severely inhibited 2 h after UV exposure but fully recovered in wild-type (WT) cells after 18 h (Fig. 3a and Extended Data Fig. 4a). The transcription recovery was completely abolished in *ELOF1* KO cells, similar to that in TC-NER-deficient *CSA* KO cells, but could be rescued by ELOF1 re-expression. Similar results were obtained by siRNA-mediated ELOF1 knockdown (Extended Data Fig. 4b,c). To distinguish whether ELOF1 has a specific function in the restart of transcription or is also involved in TBL removal, we measured TC-NER activity by quantifying the gap-filling synthesis using 5-ethynyl-2′-deoxyuridin (EdU) incorporation in non-replicating global-genomic nucleotide excision repair (GG-NER)-deficient cells[27]. Similar to CSB depletion, loss of ELOF1 severely inhibited TC-NER activity (Fig. 3b and Extended Data Fig. 4d,e). The function of ELOF1 was restricted to the TC-NER subpathway, as the gap-filling synthesis in GG-NER-proficient cells was not affected (Fig. 3c and Extended Data Fig. 4f,g). Together, this shows that ELOF1 has a crucial function in TC-NER to subsequently promote transcription recovery.

Then, we tested the sensitivity of *ELOF1* KO cells to other types of DNA damage. *ELOF1* KO cells, like *CSB* KO cells, displayed severe sensitivity to a wide spectrum of genotoxins that cause TBLs, including illudin S[28], cisplatin[29], camptothecin[30] and oxidative lesions[31] (Fig. 3d,e and Extended Data Fig. 4h–j). However, *ELOF1* KO cells were not sensitive to replication stress induced by hydroxyurea or aphidicolin (Extended Data Fig. 4k,l). Importantly, depletion of elongation factors does not generally induce sensitivity to TBLs. For example, knockdown of the elongation factors SPT4 and SPT5 did not induce UV sensitivity, although it did reduce RNA synthesis to a similar extent to that of ELOF1 depletion (Extended Data Figs. 3c–e and 4m).

ELOF1 is an evolutionarily conserved TC-NER factor. As *ELOF1* is highly conserved from archaea to mammals[15], we tested whether the *ELOF1* orthologues in *Saccharomyces cerevisiae* and *Caenorhabditis elegans* are also involved in TC-NER. Similar to

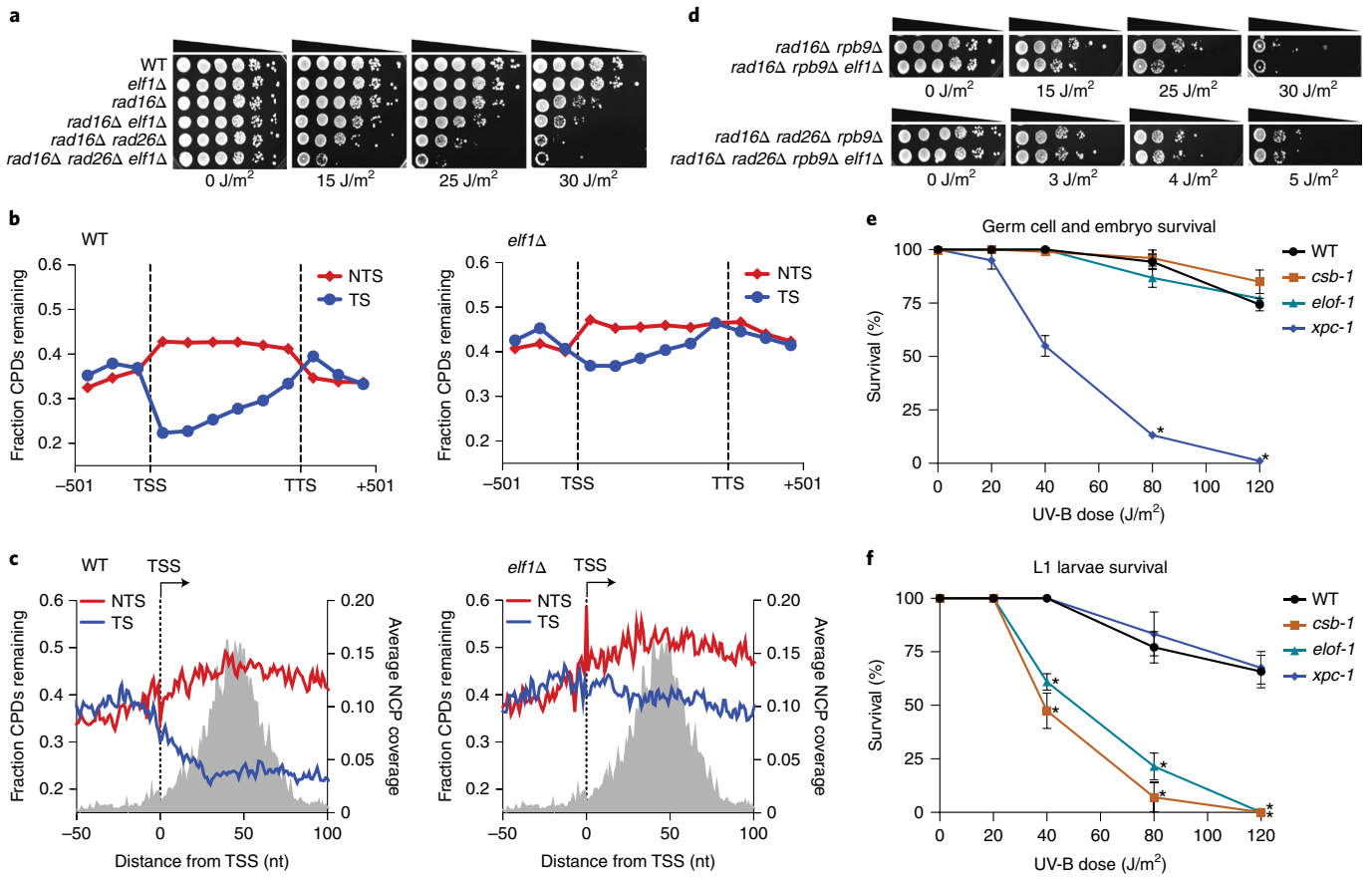

Fig. 4 | ELOF1 is an evolutionarily conserved TC-NER factor. a, Indicated mutant yeast strains were serially tenfold diluted, spotted and exposed to the indicated UV doses. The spot assays were performed three times, with similar results obtained. **b**, CPD-seq analysis of WT (left) and *elf1*Δ mutant (right) yeast showing the average fraction of unrepaired CPDs remaining on the TS and NTS for ~5,000 yeast genes following 2-h repair relative to no repair. Each gene was divided in six equally sized bins. Repair in flanking DNA upstream of the TSS and downstream of the TTS is also depicted. **c**, Close-up of CPD-seq repair data near the TSS in WT (left) and *elf1*Δ mutant (right) cells. Nucleosome positioning data[51] are shown for reference. CPD-seq was executed once. **d**, Indicated mutant yeast strains were serially tenfold diluted, spotted and exposed to the indicated UV doses. The spot assay was performed three times, with similar results obtained. **e**, *C. elegans* germ cell and embryo UV survival assay, measuring GG-NER activity, of WT, *csb-1*, *xpc-1* and *elof-1* animals. The percentages of hatched eggs (survival) are plotted against the applied UV-B doses. **f**, L1 larvae UV survival assay, measuring TC-NER activity, of WT, *csb-1*, *xpc-1* and *elof-1* animals. The percentages of animals that developed beyond the L2 stage (survival) are plotted against the applied UV-B doses. In **e** and **f**, data show the mean survival ± s.e.m. of n = three independent experiments, each performed five times. $^{*}P \leq 0.05$, $^{****}P \leq 0.0001$. Numerical data are provided in the source data.

mutations in *RAD26*, the budding yeast orthologue of *CSB*, inactivation of *ELF1* (*elf1*Δ) had no effect on UV sensitivity (Extended Data Fig. 5a), which is explained by the efficient GG-NER machinery[32]. Therefore, we studied the effect of *elf1*Δ in TC-NER in GG-NER-deficient *RAD16* mutants (*rad16*Δ). This showed strong UV sensitivity for *elf1*Δ, similar to *rad26*Δ mutants (Fig. 4a).

To determine whether the increased UV sensitivity in the *elf1*Δ mutant is caused by a TC-NER defect, we analysed CPD repair profiles in the transcribed strand (TS) and non-transcribed strand (NTS) of yeast genes 2 h after UV exposure using high-resolution CPD sequencing (CPD-seq)[33] (Extended Data Fig. 5b). Meta-analysis of ~5,000 genes (Fig. 4b) and of individual genes (Extended Data Fig. 5c) showed that in the *elf1*Δ mutant, GG-NER-mediated repair in the NTS was hardly affected, whereas TC-NER-mediated repair in the TS was severely compromised. Global repair in the *elf1*Δ mutant was hardly affected (Extended Data Fig. 5d), which is in agreement with the fact that TC-NER-specific repair only happens in the TS of active genes. Although Elf1 was described to stimulate Pol II progression on the nucleosome[20], no nucleosome-dependent difference in TC-NER efficiency was detected in the TS in *elf1*Δ mutants (Extended Data Fig. 5e).

Strikingly, the *elf1*Δ *rad26*Δ double mutant showed an even higher UV sensitivity than the single mutants in a *rad16*Δ background, which indicates that Elf1 has functions independent of Rad26 (Fig. 4a). Close-ups of the CPD-seq data showed that repair immediately downstream of the transcription start site (TSS) was compromised in the *elf1*Δ mutant (Fig. 4c). This genomic region can be repaired in a Rad26-independent manner[34] by a Rpb9-mediated transcription-coupled repair mechanism[35], and this result suggests that Elf1 has a role in this pathway. Indeed, *elf1*Δ enhances the UV sensitivity in a *rad16*Δ *rpb9*Δ mutant but not in a *rad16*Δ *rpb9*Δ *rad26* mutant (Fig. 4d and Extended Data Fig. 5f), which indicates that Elf1 is involved in both Rad26-dependent and Rpb9-dependent repair. This was confirmed by reduced TC-NER in both *rad16*Δ *rad26*Δ and *rad16*Δ *rpb9*Δ mutants after deletion of *ELF1* (Extended Data Fig. 5g,h).

To study the role of ELOF1 in a multicellular model organism, we made use of the conservation of *ELOF1* in *C. elegans*. We assayed UV survival of mutant germ and early embryonic cells, which predominantly depends on GG-NER, and of post-mitotic first-stage larvae, which mainly depends on TC-NER[36]. Inactivation of *elof-1* (Extended Data Fig. 5i) did not increase the UV sensitivity

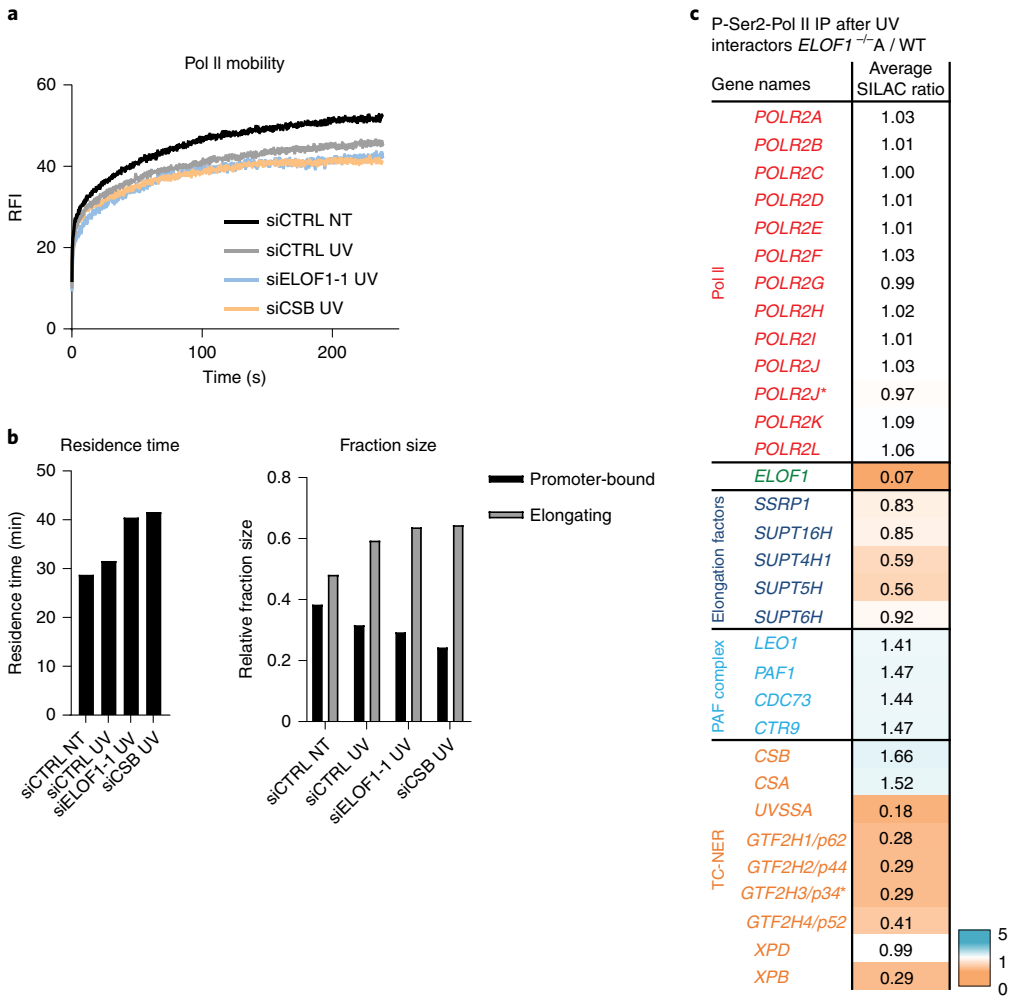

Fig. 5 | Prolonged stalling of Pol II at TBLs in the absence of ELOF1. a, FRAP analysis of Pol II mobility in MRC-5 *GFP–RPB1* KI cells after depletion of indicated factors in untreated cells or directly after UV induction (UV, 12 J/m^2). The RFI was measured over time, background-corrected and normalized to the pre-bleach fluorescence intensity. siCTRL NT $n=28$, siCTRL UV $n=30$, siELOF1-1 UV $n=17$, siCSB UV $n=24$ cells analysed across four independent experiments for siCTRL and three for siELOF1 and siCSB. **b**, Left: residence time of the elongating Pol II fraction. Right: relative fraction sizes of promoter-bound or elongating Pol II as determined by Monte-Carlo-based modelling based on the RPB1 mobility shown in **a**. **c**, Interaction heatmap based on the SILAC ratios as determined by quantitative interaction proteomics of UV-specific Pol II-interacting proteins in *ELOF1*$^{-/-}$A cells relative to WT cells. Average SILAC ratios of duplicate experiments are plotted. SILAC ratios <1 indicate loss of interaction, >1 indicate increase in interaction. Asterisk indicates proteins quantified in one experiment. Numerical data are provided in the source data.

of germ and embryonic cells, which is in contrast to inactivation of the GG-NER factor *xpc-1* (Fig. 4e). However, *elof-1* animals showed a strong UV sensitivity in the first larval stage, similar to TC-NER-deficient *csb-1* animals (Fig. 4f). These results show that ELOF1 is an evolutionarily conserved TC-NER factor.

Pol II progression is impaired in ELOF1-deficient cells after UV exposure. As the TC-NER factor ELOF1 is an integral part of the elongation complex, its depletion will probably affect Pol II progression after encountering TBLs. To test this, we used *GFP–RPB1* KI cells to study Pol II mobility by FRAP, which provides quantitative information on Pol II elongation rates and fraction sizes of elongating and promoter-bound Pol II[22]. UV-induced DNA damage increased Pol II immobilization, especially of the long-bound elongating fraction, as evident from the reduced slope of the FRAP curve at time points >100 s (ref. [22]) (Fig. 5a). Monte-Carlo-based modelling revealed an increased fraction size and residence time of elongating Pol II. This indicates that UV exposure results in more elongating Pol II that transcribes slower (Fig. 5b), which is probably caused by Pol II stalling at TBLs[37]. After knockdown of ELOF1, elongating Pol II was further immobilized following UV exposure, to a level similar as observed after CSB depletion. The average residence time of elongating Pol II in ELOF1-depleted cells increased by ~30%, which suggests that Pol II stalling at lesions is prolonged (Fig. 5a,b and Extended Data Fig. 6a). Similar results were obtained by Pol II chromatin immunoprecipitation with sequencing (ChIP-seq) experiments[38]. ELOF1 knockdown also resulted in an increased residence time of elongating Pol II in unperturbed conditions, which is indicative of a reduced elongation rate (Extended Data Fig. 6b,c); this result was in line with our DRB/TT$_{chem}$-seq data (Fig. 2e,f).

ELOF1 stimulates Pol II ubiquitylation and recruitment of UVSSA and TFIIH during TC-NER. To study TC-NER complex assembly, we performed SILAC-based interaction proteomics on P-Ser2-modified Pol II after UV exposure in the presence or absence of ELOF1. Pol II interactions with most elongation factors remained unaffected in the absence of ELOF1 (Fig. 5c, Extended

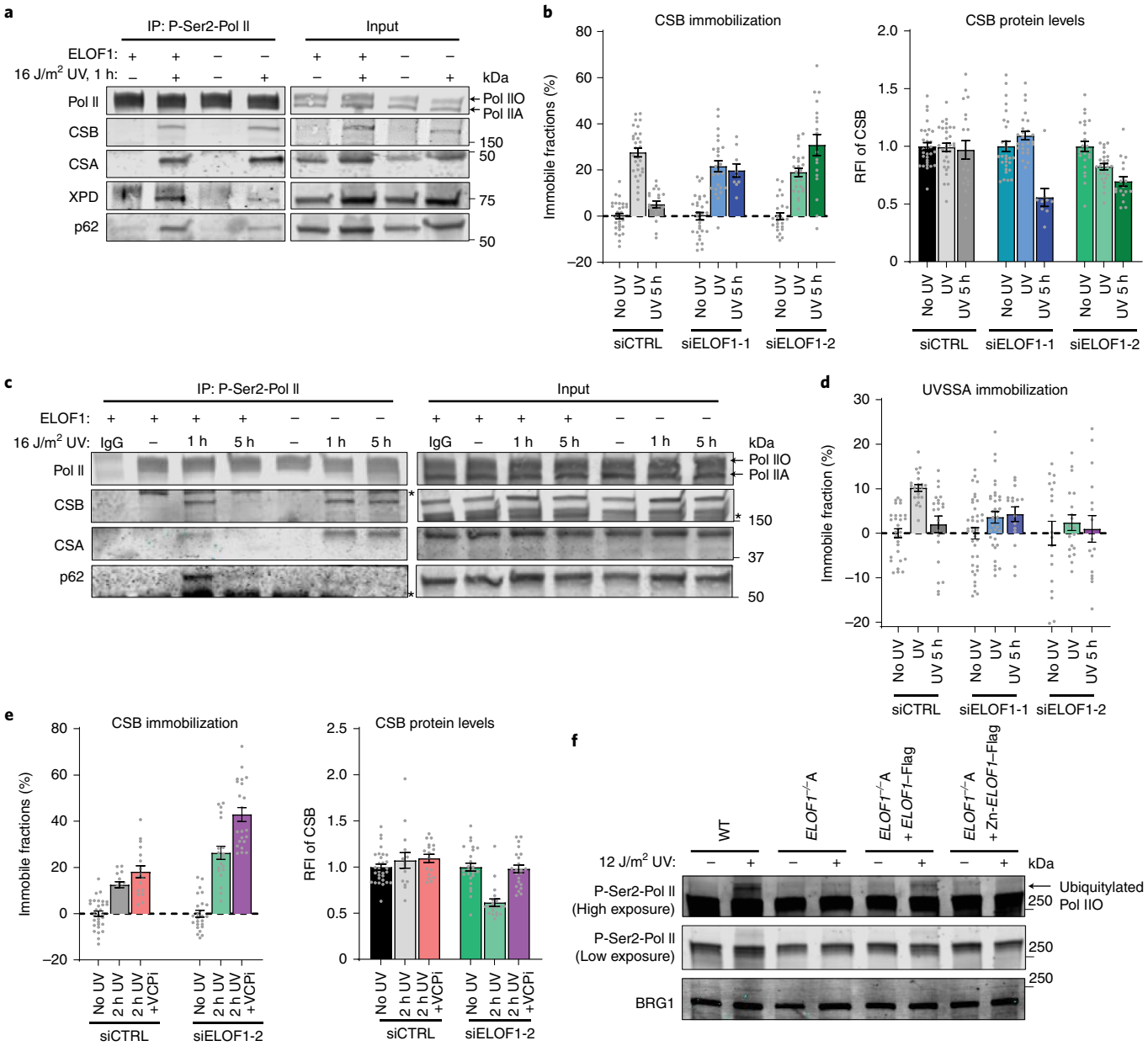

Fig. 6 | ELOF1 is crucial for proper TC-NER complex assembly. a, IP of P-Ser2-modified Pol II in WT and *ELOF*$^{-/-}$A cells followed by immunoblotting for the indicated proteins. Cells were collected 1 h after mock-treatment or irradiation with 16 J/m^2 UV. **b**, Left: relative immobile fraction of CSB in *CSB–mScarletI* KI cells transfected with the indicated siRNAs directly (UV) or 5 h after UV irradiation (5 h UV, 4 J/m^2) as determined by FRAP analysis (Extended Data Fig. 7e). Right: relative fluorescence intensity of CSB–mScarletI in *CSB* KI cells transfected with the indicated siRNAs as determined by live-cell imaging. Values represent the mean ± s.e.m. and are normalized to mock-treated. siCTRL: NT + UV $n = 30$, 5 h UV $n = 20$; siELOF1-1: NT $n = 30$, UV $n = 25$, 5 h UV $n = 9$; siELOF1-2: NT + UV $n = 25$, 5 h UV $n = 18$ cells. All were analysed from two independent experiments, except siELOF1-1 5 h UV, which was performed once. **c**, IP of P-Ser2-modified Pol II in WT and *ELOF1*$^{-/-}$A cells 1 or 5 h after UV (16 J/m^2) irradiation followed by immunoblotting for the indicated proteins. IgG was used as the binding control. Asterisk indicates a non-specific band. **d**, Same as left panel of **b** but for *UVSSA–mScarletI* KI cells (Extended Data Fig. 7f,g). siCTRL: NT $n = 30$, UV + 5 h UV $n = 21$; siELOF1-1: NT $n = 38$, UV $n = 34$, 5 h UV $n = 16$; siELOF1-2: NT + UV $n = 19$, 5 h UV $n = 16$ cells. All were analysed from two independent experiments. **e**, Relative immobile fraction (left) or relative fluorescence intensity (right) of CSB–mScarletI in *CSB* KI cells transfected with the indicated siRNAs 2 h after UV irradiation (4 J/m^2) as determined by FRAP analysis (Extended Data Fig. 7). VCPi, treatment with VCP inhibitor. Values represent the mean ± s.e.m. and are normalized to mock-treated cells. siCTRL: NT $n = 30$, 2 h UV $n = 15$, 2 h UV + VCPi $n = 17$; siELOF1-2: NT $n = 25$, 2 h UV $n = 20$, 2 h UV + VCPi $n = 22$ cells. All were analysed from two independent experiments. **f**, Immunoblot of chromatin fraction of indicated HCT116 WT or *ELOF1* KO cells, with re-expression of WT of zinc-finger mutant ELOF1, 1 h after 12 J/m^2 UV or mock treatment. Loading control was BRG1. Data shown in **a**, **c** and **f** were performed two times, with similar results obtained. Numerical data and uncropped blots are provided in the source data.

Data Fig. 6d and Supplementary Table 2). Interestingly, while CSA and CSB could still bind Pol II in the absence of ELOF1, binding of UVSSA and the TFIIH subunits was severely compromised. These results were confirmed by IP experiments (Fig. 6a), which showed that the reduced TFIIH interaction is independent of its degradation (Extended Data Fig. 6e).

Since UVSSA plays a crucial role in the recruitment of TFIIH to lesion-stalled Pol II[7,10], decreased UVSSA binding probably explains

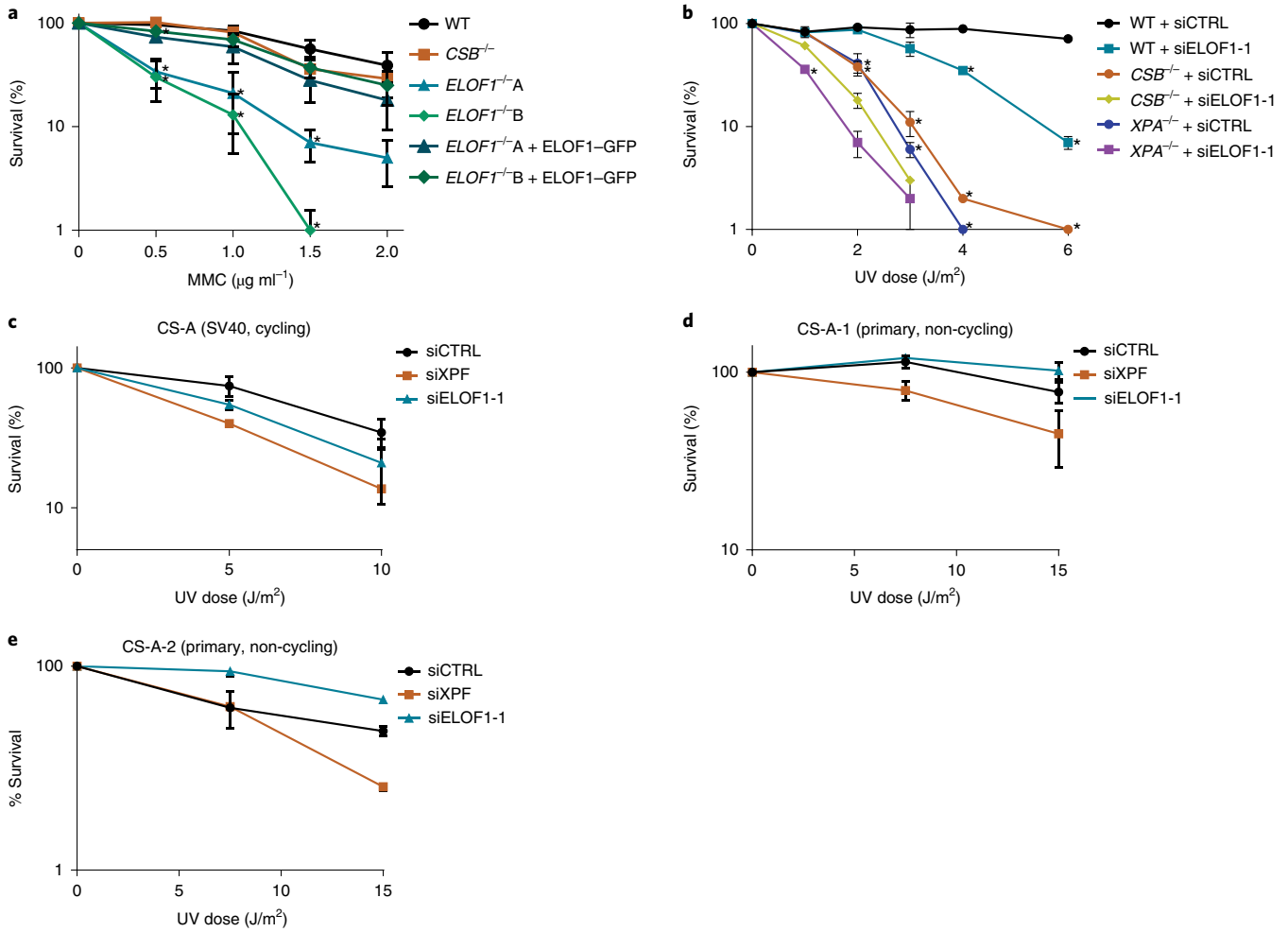

Fig. 7 | ELOF1 has an additional function apart from TC-NER. a, Relative colony survival of the indicated HCT116 WT and KO cells, with ELOF1 re-expression where indicated, after a 1-h exposure to the indicated concentrations of MMC. Plotted curves represent the mean of $n=3$ independent experiments ± s.e.m. $^*P \leq 0.05$ relative to WT analysed by one-sided unpaired *t*-test. **b**, Relative colony survival of MRC-5 WT or indicated KO cell lines, transfected with the indicated siRNAs, following exposure to the indicated doses of UV. Plotted curves represent the mean ± s.e.m. $^*P \leq 0.05$ relative to WT analysed by one-sided unpaired *t*-test. WT cells $n=4$ independent experiments, except for 1 and 3 J/m^2, which were $n=3$ independent experiments; CSB cells $n=3$ independent experiments, except for 1 and 3 J/m^2, which were $n=2$ independent experiments; XPA cells $n=3$ independent experiments. **c**–**e**, Viability of replicating CS-A (SV40) (**c**) or non-replicating primary S216LV (CS-A-1; **d**) or S1SP cells (CS-A-2; **e**) following exposure to the indicated UV doses as determined by AlamarBlue staining. Plotted curves represent the mean ± s.e.m. SV40: siCSA $n=2$ independent experiments, all other conditions $n=3$ independent experiments. hTert, CS216LV and CS1SP: $n=2$ independent experiments for all conditions. Numerical data are provided in the source data.

the reduced TFIIH recruitment and the observed TC-NER defects. To test this, we generated *CSB* and *UVSSA* KI cells (Extended Data Fig. 7a,b), expressing mScarletI-tagged CSB and UVSSA from their endogenous locus, to enable analysis of their quantity and mobility in living cells. The mobility of these factors, as determined by FRAP, is an accurate measure of their involvement in TC-NER, as shown by their UV-induced, transcription-dependent immobilization[23,39] (Extended Data Fig. 7c,d). CSB immobilization directly after UV exposure was not affected by ELOF1 depletion, which is in line with our IP experiments. However, CSB remained immobilized for up to 5 h after UV exposure (Fig. 6b and Extended Data Fig. 7e). This prolonged binding of CSB to lesion-stalled Pol II was confirmed by IP experiments that, additionally, showed prolonged binding of CSA (Fig. 6c).

In contrast to CSB, UVSSA immobilization after UV damage was severely reduced after ELOF1 depletion (Fig. 6d and Extended Data Fig. 7f,g), which further indicates that ELOF1 plays a crucial role in the recruitment of UVSSA to lesion-stalled Pol II. UVSSA recruits the deubiquitylating enzyme USP7, which protects CSB from proteasomal degradation mediated by the ubiquitin-selective segregase VCP (also known as p97)[39,40], which could explain the ~40% decreased CSB levels after UV exposure following ELOF1 depletion (Fig. 6b). Indeed, inhibition of VCP rescued CSB degradation in ELOF1-depleted cells, resulting in increased CSB immobilization after UV treatment (Fig. 6e and Extended Data Fig. 7h) and indicating that chromatin-bound CSB is degraded.

Recently, ubiquitylation of a single lysine in RPB1 (Lys1268) was described to stimulate UVSSA and TFIIH recruitment[8]. Therefore, we tested whether ELOF1 is involved in UV-induced Pol II ubiquitylation by studying the slower migrating ubiquitylated P-Ser2-modified RPB1 band[8]. *ELOF1* KO almost completely abolished UV-induced RPB1 ubiquitylation (Fig. 6f) to the same extent as *CSB* KO or inhibiting the NEDD8-conjugating enzyme NAE1, which controls the activity of CRL complexes[8,9] (Extended Data Fig. 7i). This loss of Pol II ubiquitylation was rescued by the re-expression of WT ELOF1 but not by the zinc-finger mutant. Similar results were obtained using siRNA-mediated ELOF1 depletion (Extended Data Fig. 7j). Together, these results shows that

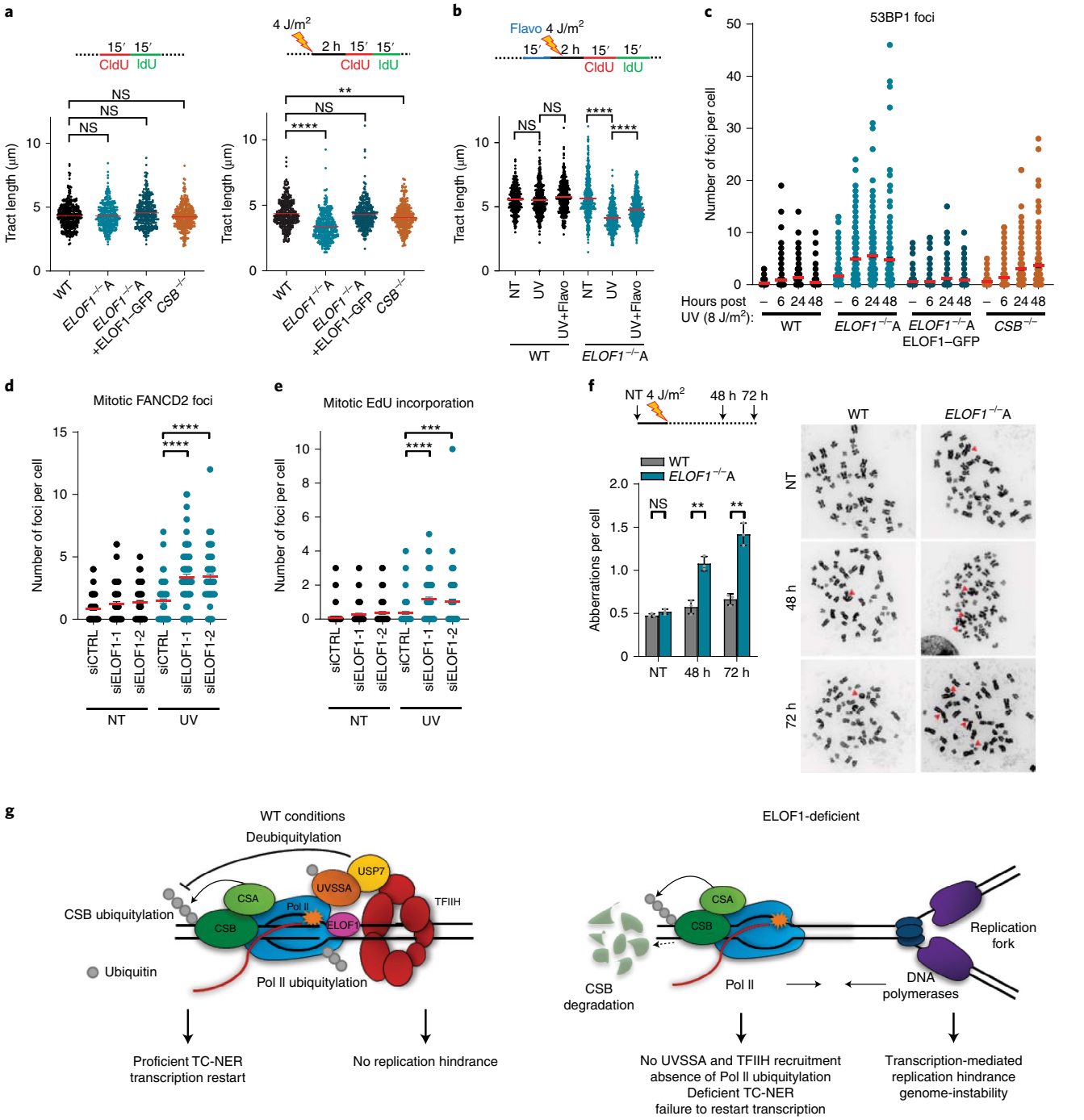

Fig. 8 | ELOF1 is important for preventing genome instability. a, Fork progression measured by tract lengths (in micrometres) of CldU in indicated HCT116 cells, in untreated conditions (left) or 2 h after 4 J/m^2 UV (right). Tracts of (left to right) $n = 347$, 343, 348, 341, 347, 335, 336 and 339 cells collected from three independent experiments. **b**, As in **a** but 2 h after 4 J/m^2 UV with or without 15 min of pretreatment with 0.1 µM flavopiridol (Flavo) of (left to right) $n = 355$, 510, 506, 506, 508 and 535 cells. **c**, Number of 53BP1 foci in the indicated HCT116 cells untreated or at the indicated time points after UV (8 J/m^2). Red lines indicate average foci number ± s.e.m. of (left to right) $n = 344$, 308, 320, 277, 292, 279, 280, 276, 279, 292, 255, 262, 330, 330, 331 and 242 cells collected from two independent experiments. **d**,**e**, Number of FANCD2 (**d**) or EdU (**e**) foci per RPE-1 *TP53*$^{-/-}$ cell transfected with the indicated siRNAs in untreated conditions or 48 h after irradiation with 4 J/m^2 UV. siCTRL NT $n = 89$, siELOF1-1 NT $n = 91$, others $n = 90$ cells analysed across three independent experiments. **f**, Left: chromosomal aberrations per cell in HCT116 WT and *ELOF1*$^{-/-}$A cells 48 or 72 h after 4 J/m^2 UV or mock treatment (NT). Data represent the mean ± s.e.m. of $n = 3$ independent experiments. Right: representative images of metaphase spreads. Arrowheads indicate chromosomal aberrations. Scale bar, 10 µm. **g**, Model showing function of ELOF1. Left: in WT conditions, ELOF1 is an integral part of the elongation complex and binds near the DNA entry tunnel and ubiquitylation site of Pol II to promote TC-NER and subsequent transcription restart, not resulting in replication problems. Right: in the absence of ELOF1, CSA and CSB are still recruited to lesion-stalled Pol II; however, UVSSA, TFIIH and Pol II ubiquitylation are absent, resulting in TC-NER deficiency and prolonged Pol II stalling, resulting in increased transcription-mediated replication hindrance and genome instability. *$P \leq 0.05$, **$P \leq 0.01$, ***$P \leq 0.001$, ****$P \leq 0.0001$, analysed by Kruskal–Wallis test for multiple comparisons (**a**,**b**), two-sided unpaired *t*-test (Mann–Whitney) (**d**,**e**) or by two-sided unpaired *t*-test with Welch's correction (**f**). Numerical data are provided in the source data.

ELOF1 is important for Pol II ubiquitylation and correct TC-NER complex assembly after DNA damage.

ELOF1 has an additional role outside TC-NER. Strikingly, while testing the sensitivity of *ELOF1* KO cells, we observed that *ELOF1* KO cells, but not *CSB* KO cells, were sensitive to the DNA crosslinker mitomycin C (MMC) (Fig. 7a). This suggests an additional function for ELOF1 in the DNA-damage response besides canonical TC-NER. The prolonged transcription block in *ELOF1* KO cells after MMC exposure (Extended Data Fig. 8a) suggests that this additional role for ELOF1 is linked to transcription. To confirm this additional function to TC-NER, we depleted ELOF1 in TC-NER-deficient *CSB* KO or NER-deficient *XPA* KO cells and observed an increased UV sensitivity (Fig. 7b). Of note, CSB also has additional functions to ELOF1 in the response to UV-induced damage (Extended Data Fig. 8b). The role of ELOF1 outside TC-NER was further shown in cells from patients with CS, which are characterized by inactivating mutations in *CSA* (CS-A), in which knockdown of ELOF1 also resulted in additional UV sensitivity (Fig. 7c). As expected, knockdown of XPF induced additional UV sensitivity in CS-A cells, as this also impedes GG-NER. Remarkably, this additive effect of ELOF1 is replication-dependent, as it was absent in non-cycling CS-A cells (Fig. 7d,e).

ELOF1 prevents transcription-mediated replication hindrance. The replication-dependent additive effect of ELOF1 to TC-NER (Fig. 7), the specific role of ELOF1 in transcription (Fig. 2) and the prolonged Pol II stalling after ELOF1 knockdown (Fig. 5a,b) suggest that lesion-stalled Pol II collides with replication forks in the absence of ELOF1. Therefore, we investigated the impact of *ELOF1* KO on DNA replication by analysing the progression of individual replication forks. Replication fork progression was not affected after *ELOF1* KO in unperturbed conditions, which indicates that ELOF1 has no role in fork progression (Fig. 8a). However, 2 h after UV exposure, the tract length was significantly decreased in *ELOF1* KO cells compared with WT cells and ELOF1-complemented cells. In *CSB* KO cells, a small effect on fork progression was observed; however, it was not to the same extent as in *ELOF1* KO cells. This suggests that loss of the elongation factor ELOF1 results in fork progression defects after induction of TBLs, which was also seen after MMC-induced DNA damage (Extended Data Fig. 8e). This is probably due to transcription-mediated replication blockage, as the effect on replication fork progression was impeded by mild transcription inhibition (Fig. 8b and Extended Data Fig. 8c), levels at which replication is not affected in unperturbed conditions (Extended Data Fig. 8d).

Transcription-replication conflicts have previously been shown to result in under-replicated DNA[2], which may cause double-strand breaks after mitotic progression and subsequently give rise to genome instability[41]. In line with this hypothesis, we observed a more pronounced increase in 53BP1 foci following UV irradiation in *ELOF1* KO cells compared with WT or *CSB* KO cells (Fig. 8c and Extended Data Fig. 8f), which was observed at all stages of the cell cycle, including in cells in G1 and G2 phase (Extended Data Fig. 8g). Furthermore, following UV exposure, we observed increased numbers of mitotic FANCD2 foci, as determined by immunofluoresence, and more mitotic DNA synthesis, as visualized by EdU incorporation after ELOF1 depletion (Fig. 8d,e and Extended Data Fig. 8h), which is indicative for under-replicated DNA[42,43]. Replication interference and under-replicated DNA are important drivers of chromosomal aberrations. In line with this, UV damage clearly resulted in an increased number of chromosomal aberrations in *ELOF1* KO cells compared with WT cells (Fig. 8f).

Discussion

We have unveiled an important and evolutionarily conserved role for ELOF1 in the cellular response to DNA-damage-induced transcription stress by two independent mechanisms: promoting TC-NER and reducing transcription-mediated replication hindrance (Fig. 8g). In line with this finding, a recent genome-wide CRISPR screen of 27 genotoxic agents identified that ELOF1 protects against different types of TBLs[44]. Interestingly, while the interaction of most TC-NER factors with elongating Pol II is strongly increased after DNA damage[1,7,23], ELOF1 is an intrinsic part of the elongating complex in unperturbed conditions, where it stimulates transcription elongation (Fig. 2). Its dual function as an elongation and repair factor can be the cause of the embryonic lethality observed in *ELOF1* KO mice[45] and may explain why, thus far, no *ELOF1* mutations have been found in TC-NER-related syndromes[4].

ELOF1 promoted UVSSA binding to lesion-stalled Pol II, resulting in subsequent TFIIH recruitment, which in turn promotes assembly of the full incision complex to excise the TBL and restart transcription. In the absence of ELOF1, TC-NER can still be initiated since CSB and CSA are properly recruited to lesion-stalled Pol II (Fig. 6). However, UVSSA is not recruited, and this suggests that more control steps are needed to recruit or stably incorporate UVSSA. This is in line with previous reports of CSA-independent UVSSA recruitment[39,46] and suggests that UVSSA recruitment is not solely mediated via a direct interaction with CSA[7,47]. Such regulation of UVSSA recruitment may represent an important proofreading step that prevents build-up of the incision complex on non-lesion-stalled Pol II. An example of such a regulatory mechanism is the recently discovered TBL-induced ubiquitylation (Lys1268) of Pol II that is crucial for Pol II stability and TFIIH recruitment[8,9]. Interestingly, based on recent structural analysis of the elongation complex in yeast[20], the Lys1268 ubiquitylation site is in close proximity of ELOF1 (Extended Data Fig. 9a,b). Since Pol II ubiquitylation depends on ELOF1, we hypothesize that ELOF1 might stimulate ubiquitylation by facilitating a correct orientation of the elongation complex or is involved in recruiting factors that promote Pol II ubiquitylation.

In addition to its role in TC-NER, our data showed that ELOF1 plays an important role in preserving genome stability after DNA damage, probably by preventing transcription-mediated replication stress (Fig. 8). Even though CSB and ELOF1 depletion had similar effects on the prolonged binding of Pol II after DNA damage (Fig. 5a), only *ELOF1* KO resulted in a clear replication defect and increased genome instability (Fig. 8). This suggests that lesion-stalled Pol II is differently processed in ELOF1-deficient cells compared with CSB-deficient cells. More research is needed to fully uncover the mechanism by which ELOF1 prevents transcription-replication conflicts and to test whether ELOF1 might also have transcription-independent functions affecting genome stability. Together, our results show that ELOF1 is an important guardian of elongating Pol II by protecting transcription from the severe consequences of TBLs via two mechanisms: stimulating repair and preventing transcription-replication conflicts.

Online content

Any methods, additional references, Nature Research reporting summaries, source data, extended data, supplementary information, acknowledgements, peer review information; details of author contributions and competing interests; and statements of data and code availability are available at https://doi.org/10.1038/s41556-021-00692-z.

Received: 24 June 2020; Accepted: 29 April 2021;
Published online: 9 June 2021

References

1. Lans, H., Hoeijmakers, J. H. J., Vermeulen, W. & Marteijn, J. A. The DNA damage response to transcription stress. *Nat. Rev. Mol. Cell Biol.* **20**, 766–784 (2019).
2. Gomez-Gonzalez, B. & Aguilera, A. Transcription-mediated replication hindrance: a major driver of genome instability. *Genes Dev.* **33**, 1008–1026 (2019).

3. Gaillard, H. & Aguilera, A. Transcription as a threat to genome integrity. *Annu. Rev. Biochem.* **85**, 291–317 (2016).
4. Laugel, V. Cockayne syndrome: the expanding clinical and mutational spectrum. *Mech. Ageing Dev.* **134**, 161–170 (2013).
5. Xu, J. et al. Structural basis for the initiation of eukaryotic transcription-coupled DNA repair. *Nature* **551**, 653–657 (2017).
6. Groisman, R. et al. CSA-dependent degradation of CSB by the ubiquitin–proteasome pathway establishes a link between complementation factors of the Cockayne syndrome. *Genes Dev.* **20**, 1429–1434 (2006).
7. van der Weegen, Y. et al. The cooperative action of CSB, CSA, and UVSSA target TFIIH to DNA damage-stalled RNA polymerase II. *Nat. Commun.* **11**, 2104 (2020).
8. Nakazawa, Y. et al. Ubiquitination of DNA damage-stalled RNAPII promotes transcription-coupled repair. *Cell* **180**, 1228–1244.e24 (2020).
9. Tufegdzic Vidakovic, A. et al. Regulation of the RNAPII pool is integral to the DNA damage response. *Cell* **180**, 1245–1261.e21 (2020).
10. Okuda, M., Nakazawa, Y., Guo, C., Ogi, T. & Nishimura, Y. Common TFIIH recruitment mechanism in global genome and transcription-coupled repair subpathways. *Nucleic Acids Res.* **45**, 13043–13055 (2017).
11. Scharer, O. D. Nucleotide excision repair in eukaryotes. *Cold Spring Harb. Perspect. Biol.* **5**, a012609 (2013).
12. Sanjana, N. E., Shalem, O. & Zhang, F. Improved vectors and genome-wide libraries for CRISPR screening. *Nat. Methods* **11**, 783–784 (2014).
13. Li, W. et al. MAGeCK enables robust identification of essential genes from genome-scale CRISPR/Cas9 knockout screens. *Genome Biol.* **15**, 554 (2014).
14. Yang, W. & Gao, Y. Translesion and repair DNA polymerases: diverse structure and mechanism. *Annu. Rev. Biochem.* **87**, 239–261 (2018).
15. Daniels, J. P., Kelly, S., Wickstead, B. & Gull, K. Identification of a crenarchaeal orthologue of Elf1: implications for chromatin and transcription in Archaea. *Biol. Direct* **4**, 24 (2009).
16. Prather, D., Krogan, N. J., Emili, A., Greenblatt, J. F. & Winston, F. Identification and characterization of Elf1, a conserved transcription elongation factor in *Saccharomyces cerevisiae*. *Mol. Cell. Biol.* **25**, 10122–10135 (2005).
17. Joo, Y. J., Ficarro, S. B., Chun, Y., Marto, J. A. & Buratowski, S. In vitro analysis of RNA polymerase II elongation complex dynamics. *Genes Dev.* **33**, 578–589 (2019).
18. Ehara, H. et al. Structure of the complete elongation complex of RNA polymerase II with basal factors. *Science* **357**, 921–924 (2017).
19. Mayer, A. et al. Uniform transitions of the general RNA polymerase II transcription complex. *Nat. Struct. Mol. Biol.* **17**, 1272–1278 (2010).
20. Ehara, H. et al. Structural insight into nucleosome transcription by RNA polymerase II with elongation factors. *Science* **363**, 744–747 (2019).
21. Steurer, B. et al. Fluorescently-labelled CPD and 6-4PP photolyases: new tools for live-cell DNA damage quantification and laser-assisted repair. *Nucleic Acids Res.* **47**, 3536–3549 (2019).
22. Steurer, B. et al. Live-cell analysis of endogenous GFP–RPB1 uncovers rapid turnover of initiating and promoter-paused RNA Polymerase II. *Proc. Natl Acad. Sci. USA* **115**, E4368–E4376 (2018).
23. van den Boom, V. et al. DNA damage stabilizes interaction of CSB with the transcription elongation machinery. *J. Cell Biol.* **166**, 27–36 (2004).
24. Gregersen, L. H., Mitter, R. & Svejstrup, J. Q. Using TTchem-seq for profiling nascent transcription and measuring transcript elongation. *Nat. Protoc.* **15**, 604–627 (2020).
25. Nudler, E. RNA polymerase backtracking in gene regulation and genome instability. *Cell* **149**, 1438–1445 (2012).
26. Jia, N. et al. A rapid, comprehensive system for assaying DNA repair activity and cytotoxic effects of DNA-damaging reagents. *Nat. Protoc.* **10**, 12–24 (2015).
27. Wienholz, F., Vermeulen, W. & Marteijn, J. A. Amplification of unscheduled DNA synthesis signal enables fluorescence-based single cell quantification of transcription-coupled nucleotide excision repair. *Nucleic Acids Res.* **45**, e68 (2017).
28. Jaspers, N. G. et al. Anti-tumour compounds illudin S and irofulven induce DNA lesions ignored by global repair and exclusively processed by transcription- and replication-coupled repair pathways. *DNA Repair (Amst.)* **1**, 1027–1038 (2002).
29. Slyskova, J. et al. Base and nucleotide excision repair facilitate resolution of platinum drugs-induced transcription blockage. *Nucleic Acids Res.* **46**, 9537–9549 (2018).
30. Veloso, A. et al. Genome-wide transcriptional effects of the anti-cancer agent camptothecin. *PLoS ONE* **8**, e78190 (2013).
31. Brooks, P. J. et al. The oxidative DNA lesion 8,5′-(*S*)-cyclo-2′-deoxyadenosine is repaired by the nucleotide excision repair pathway and blocks gene expression in mammalian cells. *J. Biol. Chem.* **275**, 22355–22362 (2000).
32. van Gool, A. J. et al. RAD26, the functional *S. cerevisiae* homolog of the Cockayne syndrome B gene *ERCC6*. *EMBO J.* **13**, 5361–5369 (1994).
33. Mao, P., Smerdon, M. J., Roberts, S. A. & Wyrick, J. J. Chromosomal landscape of UV damage formation and repair at single-nucleotide resolution. *Proc. Natl Acad. Sci. USA* **113**, 9057–9062 (2016).
34. Duan, M., Selvam, K., Wyrick, J. J. & Mao, P. Genome-wide role of Rad26 in promoting transcription-coupled nucleotide excision repair in yeast chromatin. *Proc. Natl Acad. Sci. USA* **117**, 18608–18616 (2020).
35. Li, S. & Smerdon, M. J. Rpb4 and Rpb9 mediate subpathways of transcription-coupled DNA repair in *Saccharomyces cerevisiae*. *EMBO J.* **21**, 5921–5929 (2002).
36. Lans, H. et al. Involvement of global genome repair, transcription coupled repair, and chromatin remodeling in UV DNA damage response changes during development. *PLoS Genet.* **6**, e1000941 (2010).
37. Williamson, L. et al. UV irradiation induces a non-coding RNA that functionally opposes the protein encoded by the same gene. *Cell* **168**, 843–855 e813 (2017).
38. van der Weegen, Y. et al. ELOF1 is a transcription-coupled DNA repair factor that directs RNA polymerase II ubiquitylation. *Nat. Cell Biol.* https://doi.org/10.1038/s41556-021-00688-9 (2021).
39. Schwertman, P. et al. UV-sensitive syndrome protein UVSSA recruits USP7 to regulate transcription-coupled repair. *Nat. Genet.* **44**, 598–602 (2012).
40. He, J., Zhu, Q., Wani, G., Sharma, N. & Wani, A. A. Valosin-containing protein (VCP)/p97 segregase mediates proteolytic processing of Cockayne syndrome group B (CSB) in damaged chromatin. *J. Biol. Chem.* **291**, 7396–7408 (2016).
41. Lukas, C. et al. 53BP1 nuclear bodies form around DNA lesions generated by mitotic transmission of chromosomes under replication stress. *Nat. Cell Biol.* **13**, 243–253 (2011).
42. Minocherhomji, S. et al. Replication stress activates DNA repair synthesis in mitosis. *Nature* **528**, 286–290 (2015).
43. Schoonen, P. M. et al. Progression through mitosis promotes PARP inhibitor-induced cytotoxicity in homologous recombination-deficient cancer cells. *Nat. Commun.* **8**, 15981 (2017).
44. Olivieri, M. et al. A genetic map of the response to DNA damage in human cells. *Cell* **182**, 481–496.e21 (2020).
45. Tellier, A. P., Archambault, D., Tremblay, K. D. & Mager, J. The elongation factor Elof1 is required for mammalian gastrulation. *PLoS ONE* **14**, e0219410 (2019).
46. Wienholz, F. et al. FACT subunit Spt16 controls UVSSA recruitment to lesion-stalled RNA Pol II and stimulates TC-NER. *Nucleic Acids Res.* **47**, 4011–5025 (2019).
47. Fei, J. & Chen, J. KIAA1530 protein is recruited by Cockayne syndrome complementation group protein A (CSA) to participate in transcription-coupled repair (TCR). *J. Biol. Chem.* **287**, 35118–35126 (2012).
48. Evers, B. et al. CRISPR knockout screening outperforms shRNA and CRISPRi in identifying essential genes. *Nat. Biotechnol.* **34**, 631–633 (2016).
49. Nilson, K. A. et al. THZ1 reveals roles for Cdk7 in co-transcriptional capping and pausing. *Mol. Cell* **59**, 576–587 (2015).
50. Chao, S. H. et al. Flavopiridol inhibits P-TEFb and blocks HIV-1 replication. *J. Biol. Chem.* **275**, 28345–28348 (2000).
51. Weiner, A. et al. High-resolution chromatin dynamics during a yeast stress response. *Mol. Cell* **58**, 371–386 (2015).

Methods

Cell lines and cell culture. MRC-5 (SV40) immortalized human lung fibroblast cells and HCT116 colorectal cancer cells were cultured in a 1:1 mixture of DMEM (Gibco) and Ham's F10 (Invitrogen) supplemented with 10% fetal calf serum (FCS; Biowest) and 1% penicillin–streptomycin in a humidified incubator at 37 °C and 5% CO_2. C5RO fibroblasts (hTert), CS3BE (CS-A, SV40), XP186LV (XP-C), CS1SP (CS-A, primary) and CS216LV (CS-A, primary) cells were maintained in Ham's F10 with 15% FCS and antibiotics.

For SILAC, cells were grown for 2 weeks (>10 cell doublings) in arginine/lysine-free SILAC DMEM (ThermoFisher) supplemented with 15% dialysed FCS (Gibco), 1% penicillin–streptomycin, 200 µg ml^{-1} proline (Sigma) and either 73 µg ml^{-1} light [$^{12}C_6$]-lysine and 42 µg ml^{-1} [$^{12}C_6$, $^{14}N_4$]-arginine (Sigma) or heavy [$^{13}C_6$]-lysine and [$^{13}C_6$, $^{15}N_4$]-arginine (Cambridge Isotope Laboratories).

HCT116 KO cells were generated by transiently transfecting HCT116 cells with a pLentiCRISPR.v2 plasmid[12] containing appropriate sgRNAs. Transfected cells were selected using 1 µg ml^{-1} puromycin (Invitrogen) for 2 days, and single cells were seeded to allow expansion. Genotyping of single-cell clones was performed by immunoblotting or genomic PCR as indicated. sgRNA sequences are presented in Supplementary Table 4.

ELOF1 complemented cell lines were generated by lentiviral transduction in *ELOF1*$^{-/-}$ cells. Therefore, full-length expression constructs with ELOF1–Flag–GFP or WT or mutated ELOF1–Flag were synthesized (Genscript). For ΔN-ELOF1–Flag, the first 15 amino acids were deleted. For Zn-ELOF1–Flag, amino acids 26 and 29 were mutated from a cysteine to a serine (TGC to TCC). Tagged ELOF1 constructs were inserted in a pLenti-CMV-puro-DEST plasmid[52]. After transduction, cells were selected with 1 µg ml^{-1} puromycin.

HCT116 osTIR1 KI cells[53] were generated by transiently transfecting cells with a sgRNA-containing pLentiCRISPR.v2 plasmid (sgRNA sequences in Supplementary Table 4) targeting the stop codon of *ELOF1*, *CSB* or *UVSSA* and co-transfecting a homology-directed repair template, which included an auxin-inducible degron, a fluorescent mScarletI tag, a HA tag, a hygromycin -resistance cassette and homology arms (140 bp for *ELOF1*, 200 bp for *CSB* and *UVSSA*, sequences upon request)[54]. Subsequently, cells were seeded at a low density to allow expansion and were kept in the presence of 100 µg ml^{-1} hygromycin for 2 weeks to select for successful recombination. Single-cell clones were genotyped, and homozygous KI clones were selected for further analysis. A *GFP–RPB1* KI was generated in HCT116 WT or ELOF1-KI cells as previously described by Steurer et al.[22]. MRC-5 *GFP–RPB1* KI cells[22] expressing CPD-PL–mCherry were generated as previously described[21].

Genotyping PCR was performed on genomic DNA (isolated using a PureLink Genomic DNA Mini kit according to the manufacturer's protocol) with Phusion (NEB) or Taq (Invitrogen) polymerases according to the manufacturer's protocol. Primer sequences are provided in Supplementary Table 4. If necessary for assessing genomic alterations, PCR fragments were sequenced with forward primers and indels were analysed using TIDE analysis[55].

siRNA transfections were performed 2 or 3 days before each experiment using Lipofectamine RNAiMax (Invitrogen) according to the manufacturer's protocol. The following siRNAs were purchased from Dharmacon: siELOF1-1: 5′-CCGUG UGCCUAGAGGAAUUUU-3′; siELOF1-2: 5′- GAAAUCCUGUGAUGUGAAA UU-3′; siCSB: 5′-GCAUGUGUCUUACGAGAUAUU-3′; siXPF: M-019946-00; siSPT4: L-012602-00-0005; siSPT5: L-016234-00-0005; and siCSA: L-011008-00-0005. Knockdown efficiency was determined by immunoblotting or quantitative PCR with reverse transcription (RT–qPCR).

For UV (UV-C) irradiation, cells were washed with PBS and placed under a 254-nm germicidal UV-C lamp (Philips). The duration of irradiation was controlled with an air-pressured shutter connected to a timer, and cells were irradiated with doses as indicated. Cells were treated with a VCP inhibitor (Seleck Chemicals, 5 µM) directly after UV irradiation or pretreated 1 h before irradiation with the proteasome inhibitor MG132 (Enzo, 50 µM) or the NEDD8 E1 activating enzyme inhibitor MLN4924 (R&D Systems, 10 µM) where indicated. Cells were treated for 1 h with the following chemicals: flavopiridol (Sigma, 1 µM), THZ1 (Xcessbio, 2 µM), MMC (Sigma, 10 µg ml^{-1} unless indicated differently) or potassium bromate ($KBrO_3$, Sigma). Cells were continuously exposed to camptothecin or treated for 24 h with cisplatin, illudin S or hydroxyurea (all from Sigma). The final concentrations of all inhibitors were diluted in culture medium and cells were washed once with PBS before putting fresh medium after removing the damaging agent when necessary. For ionizing radiation, plates were irradiated using a RS320 X-ray cabinet (X-Strahl). For photoreactivation, cells were washed with PBS and covered with a thin layer of HBSS (ThermoFisher) before exposing them to white-light tubes (General Electric Lighting Polylux LX F36W/840) for 10 min at 37 °C[21]. Mock-treated samples were covered with tinfoil during photoreactivation.

GeCKO v2 lentiviral library production and transduction. We used the lentiCRISPRv2 human library designed by Shalem et al.[56] and obtained from Addgene. The sgRNA library was synthesized using array synthesis as previously described[56] and cloned as a pool into the lentiCRISPR transfer plasmid for virus production.

To produce the pooled lentiviral library, 12 T-225 flasks of HEK293T cells were seeded at ~40% confluency the day before transfection. Per flask, 10 µg of pVSVg, 15 µg of psPAX2 (Addgene) packaging plasmids and 20 µg of lentiCRISPR plasmid library were transfected using Lipofectamine 2000 and Plus reagent (Life Technologies) according to the manufacturer's instructions. After 6 h, the medium was changed, and after 60 h, the medium was collected and centrifuged at 3,000 r.p.m. for 10 min at 4 °C to pellet cell debris. The supernatant was filtered through a 0.45-µm low-protein-binding membrane (Millipore Steriflip HV/PVDF). To achieve a 300 times concentration of the GeCKO pooled library, the virus was ultracentrifuged (Sorvall) at 24,000 r.p.m. for 2 h at 4 °C and then resuspended overnight at 4 °C in D10 supplemented with 1% BSA. Aliquots were stored at −80 °C.

Per condition, 20 million MRC-5 cells were transduced at 75% confluency in 145-cm^2 dishes with concentrated lentivirus diluted in 18 ml of culture medium supplemented with 12 µg ml^{-1} polybrene (Sigma). The virus titre was determined to achieve a multiplicity of infection of <0.25. The next day, cells were re-seeded at 25% confluency in culture medium containing 2 µg ml^{-1} puromycin. Cells were expanded for 1 week in puromycin-containing medium. The culture medium was refreshed every other day.

Genome-wide CRISPR screen. For UV irradiation or mock treatment, 30 million transduced and puromycin-selected cells were seeded per condition at 40% confluency in 145-cm^2 dishes (2.25 million cells per dish) in medium without puromycin. The next day (day 0), dishes were mock-treated or irradiated with 6.8 J/m^2 UV-C. Control cells (mock-treated) and UV irradiated cells were washed with PBS and (mock) irradiated every day for ten consecutive days. The culture medium was refreshed after each irradiation. Mock-treated cells were reseeded to 40% confluency when they reached a confluency >90%. After the last irradiation, cells were given 24 h to recover and genomic DNA was isolated using a Blood & Cell Culture DNA Midi kit (Qiagen) according to the manufacturer's protocol (DNA content of MRC-5 cells was estimated at 10 pg per cell, genomic DNA from a maximum of 15 million cells was loaded per column). The screen was performed in duplicate.

PCR and next-generation sequencing. Per condition, sgRNA sequences of at least 300 µg of DNA (from ~30 million cells) were amplified by PCR (PCR1) using barcoded forward primers to be able to deconvolute multiplexed samples after next-generation sequencing (primers and barcodes are listed in Supplementary Table 4). PCR1 was performed using 3 µg of genomic DNA in a total volume of 50 µl per reaction. Each PCR1 reaction contained 1 U of Phusion Hot Start II polymerase (Thermo Fisher Scientific), 1× reaction buffer, 200 nm of each dNTP, 0.5 µM of both forward and reverse primer and 3% dimethylsulfoxide. The following PCR program was used: initial denaturation for 3 min at 98 °C; 35 cycles of denaturation for 1 s at 98 °C; primer annealing for 30 s at 60 °C; extension for 30 s at 72 °C; and final extension of 10 min at 72 °C. Individual PCR reaction products were pooled per condition, and 2 µl of pooled PCR product was used for a second PCR (PCR2) using primers containing adapters for next-generation sequencing (Supplementary Table 4). The same PCR program was used as for PCR1, except that only 15 cycles were applied. A total of 30 µl of PCR2 product was cleaned up to remove primer pairs using a NucleoSpin Gel & PCR clean up kit (Bioké). Equal DNA content between conditions was checked by gel electrophoresis, and samples were equimolarly pooled and subjected to Illumina next-generation sequencing as described before[48]. Mapped read-counts were subsequently used as input for the MAGeCK analysis software package (v.0.5). For each condition, two biological replicates were performed. All conditions were simultaneously sequenced. To determine which genes showed a significant negative selection after 10 days of UV treatment, the sequencing data were analysed with the MAGeCK tool[13]. GO term enrichment analysis was performed using the g:Profiler website. Genes with a FDR < 0.1 were analysed and the top ten biological processes affected by UV treatment were identified.

Survival assays. For the clonogenic survival assay, 200–300 cells were seeded per well in triplicate in a 6-well plate. The following day, cells were treated with different DNA-damaging agents. Following treatment, colonies were grown for 7–10 days, after which they were fixed and stained using Coomassie blue (50% methanol, 7% acetic acid and 0.1% Coomassie blue (all Sigma)). To assess the growth speed of siRNA-transfected cells, 10,000 (HCT116) or 20,000 (*ELOF1*$^{-/-}$A) cells were seeded in a 6-well plate and grown for 10 days after transfection. Colony numbers were counted using GelCount (Oxford Optronix). The relative colony number was plotted from at least two independent experiments, each performed in triplicate. Levels were normalized to mock-treated, set to 100 and plotted with s.e.m. values. Statistics was performed using independent *t*-tests.

For the AlamarBlue survival assay, siRNA-transfected cells were seeded to confluency in the presence of 0.5% serum in triplicate in 96-well plates to arrest cells in G0 and UV-irradiated after 30 h. After 72 h of UV irradiation, AlamarBlue (Invitrogen) was added for 4 h and the fluorescence was measured at 570 nm using a SpectraMax iD3 reader. Data were background-corrected and normalized to mock-treated conditions.

RNA isolation, complementary DNA synthesis and RT–qPCR. To determine *ELOF1* expression levels, RNA was isolated using a RNeasy mini kit (Qiagen) and

cDNA was synthesized using SuperScript II reverse transcriptase (Invitrogen), both according to the manufacturer's protocol. The generated cDNA was amplified either by standard RT–qPCR using SYBR green or amplified performing the TaqMan assay and run on a CFX96 Touch Real-Time PCR detection system (Bio-Rad).

For standard RT–qPCR, PowerUp SYBR green master mix (Thermo Fisher) was used according to the manufacturer's protocol. Samples were loaded in triplicate and the following program was used: 50 °C for 2 min; 95 °C for 2 min; 45 cycles of 15 s at 95 °C and 1 min at 58 °C followed by a dissociation curve; 95 °C for 10 s and heating from 65 °C to 95 °C with an increment of 0.5 °C, 5 s each. Data collection was enabled at each increment of the dissociation curve. For the TaqMan assay, the generated cDNA was amplified using 1× TaqMan assay (ELOF1: Hs00361088_g1, GAPDH: 4333764T, both from ThermoFisher) and 1× TaqMan gene expression master mix (ThermoFisher) by activating UNG for 2 min at 50 °C, activating the polymerase for 10 min at 95 °C, followed by 40 cycles of 15 s of denaturing at 95 °C and 1 min of annealing and extending at 60 °C in a CFX96 Touch Real-Time PCR detection system. mRNA expression levels were normalized to *GAPDH* using the $2^{-\Delta\Delta c_t}$ method[57].

Cell lysis and immunoblotting. Cells were directly lysed in SDS–PAGE loading buffer (0.125 M Tris pH 6.8, 2% SDS, 0.005% bromophenol blue, 21% glycerol and 4% β-mercaptoethanol) or, for assessing the chromatin fraction, one confluent 9.6-cm^2 dish was lysed for 30 min at 4 °C in buffer containing 30 mM HEPES pH 7.5, 130 mM NaCl, 1 mM $MgCl_2$, 0.5% Triton X-100, complete EDTA-free protease inhibitors (Roche), phosphatase inhibitor cocktail 2 (Sigma), *N*-ethylmaleimide (Sigma) and 50 μM MG132i. Chromatin was pelleted at 15,000 RPM for 10 min at 4 °C and washed once. Finally, the chromatin was digested for 30 min at 4 °C in presence of 50 U of benzonase (Millipore) before adding SDS–PAGE loading buffer and incubating for 5 min at 95 °C. Chromatin fractions or cell lysates were separated on 4–15% Mini-Protean TGX precast protein gels (Bio-Rad). Proteins were transferred onto polyvinylidenedifluoride membranes (0.45 μm, Merck Millipore) at 4 °C either for 1.5 h at 90 V with 1× transfer buffer (25 mM Tris, 190 mM glycine and 10% methanol) or overnight at 25 V in 2× transfer buffer (50 mM Tris and 380 mM glycine). Membranes were blocked with 5% BSA (Sigma) in PBS–Tween (0.05%) and probed with primary antibodies (Supplementary Table 3). Subsequently, membranes were extensively washed with PBS–Tween and incubated with secondary antibodies coupled to IRDyes (LI-COR; Supplementary Table 3) to visualize proteins using an Odyssey CLx infrared scanner (LI-COR).

FRAP. For FRAP, a Leica TCS SP5 microscope (LAS AF software, Leica) equipped with a HCX PL APO CS ×63 1.40 NA oil-immersion lens (for ELOF1, RPB1 and CSB) or a Leica TCS SP8 microscope (LAS AF software, Leica) equipped with a HC PL APO CS2 ×63 1.40 NA oil-immersion lens (for UVSSA) was used. Cells were maintained at 37 °C and at 5% CO_2 during imaging. A narrow strip of 512 × 32 pixels (for ELOF1 and RPB1) or 512 × 16 (for CSB and UVSSA) spanning the nucleus was imaged every 400 ms (200 ms for UVSSA during pre-bleaching) at 400 Hz using a 488-m laser (RPB1) or 561-nm laser (ELOF1, CSBand UVSSA). A total of 25 (RPB1), 40 (ELOF1) or 5 (CSB and UVSSA) frames were measured to reach steady-state levels before photobleaching (one frame 100% laser power for RPB1 and ELOF1, two frames for CSB and UVSSA). After photobleaching, the recovery of fluorescence was measured with 600 (ELOF1 and RPB1), 40 (CSB) or 20 (UVSSA) frames until steady-state was reached. Fluorescence intensity was measured inside and outside the nucleus, and recovery was determined by correcting for the background signal and normalizing the values to the average pre-bleach fluorescence intensities. Relative fluorescence intensity levels were calculated using the pre-bleach intensities corrected for background. Immobile fractions (F_{imm}) were calculated using the individual and average (indicated by <brackets>) fluorescence intensities after bleaching (I_{bleach}) and fluorescence intensities after recovery from the bleaching ($I_{recovery}$) as follows:

$$F_{imm} = 1 - (I_{recovery,UV} - < I_{bleach} >)/(I_{recovery,unc} > - < I_{bleach} >)$$

Experimental FRAP curves of Pol II were simulated using Monte-Carlo-based computational modelling as previously described[22] to determine the residence time of elongating Pol II and the fraction size of promoter-bound and elongating Pol II.

Native IP. Cells were mock-treated or irradiated with 16 J/m^2 UV-C 1 h before cell collection. Cell pellets were prepared from three confluent 145-cm^2 dishes per condition for IP followed by immunoblotting or eight confluent 145-cm^2 dishes per condition for mass spectrometry. Cells were collected by trypsinization and pelleted in cold PBS by centrifugation for 5 mins at 1,500 r.p.m. After one wash with cold PBS, cell pellets were stored at −80 °C until IP analysis.

For IP, pellets were thawed on ice and lysed for 20 min at 4 °C in HEPES buffer containing 30 mM HEPES pH 7.6, 1 mM $MgCl_2$, 150 mM NaCl, 0.5% NP-40 and 1× complete EDTA-free protease inhibitor cocktail (Roche). Chromatin was pelleted by spinning for 5 min at 10,000 × *g* at 4 °C and subsequently incubated for 1 h at 4 °C in HEPES buffer containing 500 U of benzonase (Millipore) and 2 μg Pol II antibody (ab5095, Abcam) or IgG (sc2027, Santa Cruz) to digest the chromatin. After 1 h, the NaCl was increased to 300 mM to inactivate benzonase, and antibody binding was continued for another 30 min. The undigested fraction was pelleted at 13,200 r.p.m. for 10 min at 4 °C, and the soluble, antibody-bound fraction was immunoprecipitated for 90 min at 4 °C using 25 μl slurry salmon sperm protein A agarose beads (Millipore). Unbound proteins were removed by washing the beads five times in wash buffer (30 mM HEPES pH 7.6, 150 mM NaCl, 1 mM EDTA, 0.5% NP-40 and 0.2× complete EDTA-free protease inhibitor cocktail). Bound proteins were eluted in SDS–PAGE loading buffer and separated on 4–15% Mini-Protean TGX precast protein gels (Bio-Rad). Samples were processed for immunoblotting or fixed and stained for mass spectrometry using Imperial protein stain (Pierce) according to the manufacturer's protocol.

For ELOF1 IP, the same protocol was followed but instead of adding antibody during chromatin digestion, precipitation was performed using RFP-Trap agarose beads (Chromotek) and binding control agarose beads (Chromotek).

Crosslinked IP. Cells were mock-treated or irradiated with 16 J/m^2 UV-C 1 h before cell collection. Cell pellets were prepared from eight confluent 145-cm^2 dishes per condition for mass spectrometry. MRC-5 *GFP–RPB1* KI cells were used for Pol II IP (Flag-beads) and HCT116 *ELOF1* KI cells were used for ELOF1 IP (HA-beads).

Crosslinked IP was performed as previously described[46] with modifications as indicated. Cells were crosslinked with 1% paraformaldehyde in serum-free DMEM for 7 min with constant shaking before quenching the reaction for 5 min with glycine (final concentration of 0.125 M). Cells were collected by scraping in PBS with 10% glycerol and 1 mM phenylmethylsulfonyl fluoride and pelleted for 15 min at maximum speed at 4 °C. Consequently, chromatin was purified by washing the cell pellets for 30 min at 4 °C in buffer 1 (50 mM HEPES, 150 mM NaCl, 1 mM EDTA, 0.5 mM EGTA, 0.25% Triton X-100, 0.5% NP-40 and 10% glycerol), pelleting the cells for 10 min at 1,300 r.p.m., washing the pellet twice with buffer 2 (10 mM Tris pH 8.0, 200 mM NaCl, 1 mM EDTA and 0.5 mM EGTA) and finally pelleting the chromatin, all at 4 °C. Chromatin was sonicated in RIPA buffer (10 mM Tris pH 7.5, 150 mM NaCl, 5 mM EDTA, 0.1% SDS, 1% sodium deoxycholate and 0.5 mM EGTA) using a Bioruptor sonicator (Diagenode) with 14 cycles of 15 s on/15 s off using the highest amplitude. Extracted chromatin was collected by spinning for 15 min at maximum speed and pre-cleared for 30 min with Protein G agarose beads (Pierce) at 4 °C. IP was performed by incubating for 4 h at 4 °C with Flag M2 agarose beads (Sigma). Finally, nonspecific interactors were removed by washing five times with RIPA buffer, and proteins were eluted and crosslinking was reversed by incubating for 30 min at 95 °C in SDS–PAGE loading buffer. Samples were separated on 4–15% Mini-Protean TGX precast protein gels (Bio-Rad) and fixed and stained using Imperial protein stain in preparation of mass spectrometry. To all buffers, 1 mM phenylmethylsulfonyl fluoride, 0.5 mM Na_2VO_4, 5 mM NaF, 5 mM NaPPi, 10 mM β-glycerol and complete EDTA-free protease inhibitor cocktail were added.

For ELOF1 IP, the same protocol was followed but with minor alterations. Cells were crosslinked in 1 mM dithiobis(succinimidyl propionate) in PBS for 30 min and quenched by adding Tris pH 7.5 to a final concentration of 25 mM for 10 min. IP was performed using HA-agarose beads (Sigma), and beads were incubated for 5 min at 95 °C to elute and reverse crosslinked immunocomplexes.

Mass spectrometry. SDS–PAGE gel lanes were cut into slices and subjected to in-gel reduction with dithiothreitol (Sigma, D8255), alkylation with iodoacetamide (Sigma, I6125) and digestion with trypsin (sequencing grade; Promega) as previously described[39]. Nanoflow liquid chromatography–tandem mass spectrometry (nLC–MS/MS) was performed on an EASY-nLC 1200 coupled to a Lumos Tribid Orbitrap mass spectrometer (ThermoFisher Scientific) operating in positive mode. Peptide mixtures were trapped on a 2 cm × 100 μm Pepmap C18 column (Thermo Fisher, 164564) and then separated on an in-house packed 50 cm × 75 μm capillary column with 1.9-μm Reprosil-Pur C18 beads (Dr. Maisch) at a flow rate of 250 nl min^{-1} using a linear gradient of 0–32% acetonitrile (in 0.1% formic acid) over 90 min. The eluate was directly sprayed into the electrospray ionization source of the mass spectrometer. Spectra were acquired in continuum mode; fragmentation of the peptides was performed in data-dependent mode by HCD. Mass spectrometry data were analysed using MaxQuant software (v.1.6.3.3). The FDR of both PSM and protein was set to 0.01, and the minimum ratio count was set to 1. The Andromeda search engine was used to search the MS/MS spectra against the UniProt database (taxonomy: *Homo sapiens*, release June 2017), concatenated with the reversed versions of all sequences. A maximum of two missed cleavages was allowed. In case the identified peptides of two proteins were the same or the identified peptides of one protein included all peptides of another protein, these proteins were combined by MaxQuant and reported as one protein group. Before further analysis, known contaminants and reverse hits were removed. GO term enrichment analysis was performed using the g:Profiler website. Genes with an average SILAC ratio of >2.5 were analysed, and the top ten biological processes affected by UV were identified.

DRB/TT$_{chem}$-seq method. DRB/TT$_{chem}$-seq was carried out as described in Gregersen et al.[24] in two biological replicates. Briefly, 8 × 10^6 cells were incubated in 100 μM DRB (Sigma-Aldrich) for 3.5 h. The cells were then washed twice in PBS, and fresh DRB-free medium was added to restart transcription. The RNA was labelled in vivo with 1 mM 4SU (Glentham Life Sciences) for 10 min before the

addition of TRIzol (Thermo Fisher Scientific), which was used to stop the reaction at the desired time point. Following extraction, 100 µg of RNA was spiked-in with 1 µg 4-thiouracile-labelled *S. cerevisiae* RNA (strain BY4741, MATa, his3D1, leu2D0, met15D0, ura3D0) and then fragmented with NaOH and biotinylated with MTSEA biotin-XXlinker (Biotium). The biotinylated RNA was then purified using µMACS streptavidin microbeads (Miltenyi Biotec) and used for library preparation. The libraries were amplified using a KAPA RNA HyperPrep kit (Roche) with modifications as previously described[9]. The fragmentation step was omitted and the RNA, resuspended in FPE Buffer, was denatured at 65 °C for 5 min. Two SPRI bead purifications were carried out with a bead-to-sample volume ratio of 0.95× and 1×. The libraries were then sequenced with single-end 75 bp reads on a Hiseq4000, with ~50,000,000 reads per sample.

Computational analysis. DRB/TT$_{chem}$-seq data were processed using a previously published protocol[24]. Briefly, reads were aligned to human GRCh38 Ensembl 86. Read depth coverage was normalized to account for differences between samples using a scale factor derived from a yeast spike-in aligned and counted against *S. cerevisiae* R64-1-1 Ensembl 86 (ref. [58]). Biological replicate alignments were combined for the purpose of visualization and wave-peak analysis to increase read-depth coverage.

A set of non-overlapping protein-coding genes of >200 kb and of 50–100 kb were selected for wave-peak analysis. A meta-gene profile was calculated by taking a trimmed mean of each base-pair coverage in the region −2kb:+200 kb around the TSS. This was further smoothened using a spline. Wave peaks were called at the maximum points on the spline, with the stipulation that the peak must advance with time before being subjected to manual review. Elongation rates (kb min^{-1}) were calculated by fitting a linear model to the wave-peak positions as a function of time.

EU incorporation. Cells were grown on coverslips and transcription levels were measured by pulse labelling with EU (Jena Bioscience) in Ham's F10 medium supplemented with 10% dialysed FCS and 20 mM HEPES buffer (both Gibco). Cells were labelled for 30 min using 400 µM EU (MRC-5 cells) or for 1 h with 200 µM EU (HCT116 cells) before fixation with 3.7% formaldehyde (FA; Sigma) in PBS for 15 min at room temperature. After permeabilization with 0.1% Triton X-100 in PBS for 10 min and blocking in 1.5% BSA in PBS for 10 min, Click-it-chemistry-based azide coupling was performed by incubation for 1 h with 60 µM Atto594 Azide (Attotec) in 50 mM Tris buffer (pH 8) with 4 mM $CuSO_4$ (Sigma) and 10 mM freshly prepared ascorbic acid (Sigma). 4,6-Diamidino-2-phenylindole (DAPI; Brunschwieg Chemie) was added to visualize the nuclei. Coverslips were washed with 0.1% Triton in PBS and with PBS only and mounted with Aqua-Poly/Mount (Polysciences). Cells were imaged using a Zeiss LSM 700 Axio Imager Z2 upright microscope equipped with a ×40 Plan-apochromat 1.3 NA oil-immersion lens or ×63 Plan-apochromat 1.4 NA oil-immersion lens (Carl Zeiss Micro Imaging). The integrated density of the EU signal in the nuclei was quantified using ImageJ. Therefore, the surface of each nucleus was determined based on the DAPI signal, and the mean fluorescence intensity was determined, corrected for the background signal. With these values, the integrated density was calculated and plotted as single-cell points with the average and s.e.m.

For assessing recovery of transcription after UV exposure, cells were mock-treated or irradiated with 8 J/m^2 UV-C for 2 or 18 h before EU incorporation. For recovery after MMC treatment, cells were mock-treated or incubated for 2 h with 10 µg ml^{-1} MMC followed by a recovery period of 2 or 22 h in normal medium. Integrated density was normalized to mock-treated cells.

TC-NER-specific unscheduled DNA synthesis. Amplified unscheduled DNA synthesis (UDS) was performed as previously described[27]. Briefly, siRNA-transfected primary XP186LV (XP-C patient cells) were serum-deprived for at least 24 h in Ham's F10 (Lonza) containing 0.5% FCS and antibiotics to arrest cells in G0. Cells were irradiated using 8 J/m^2 UV and labelled for 7 h with 20 µM NCP (EdU) and 1 µM floxuridine (Sigma). Subsequently, a 15-min chase was performed with normal medium (0.5% FCS) supplemented with 10 µM thymidine (Sigma) to remove unincorporated EdU, and cells were fixed and permeabilized with 3.7% FA and 0.5% Triton X-100 for 15 min. After permeabilizing the cells for 20 min with 0.5% Triton in PBS and washing with 3% BSA in PBS, endogenous peroxidase activity was quenched using 2% hydrogen peroxide (Sigma) for 15 min and incubated with PBS+ (0.5% BSA and 0.15 % glycine). Click-it chemistry was performed using the Click-it reaction cocktail containing azide–PEG3–biotin conjugate (20 µM, Jena Bioscience), 1× Click-it reaction buffer (ThermoFisher Scientific), copper(III) sulfate (0.1 M) and 10× reaction buffer additive (ThermoFisher Scientific) for 1 h and washed with PBS. To amplify the signal, coverslips were incubated for 1 h using HRP–streptavidin conjugate (500 µg ml^{-1}) followed by PBS washes and a 10-min incubation with Alexa-Fluor-488-labelled tyramide (100× stock, ThermoFisher Scientific). Coverslips were washed with PBS and PBS+ and the nuclei were stained with DAPI in 0.1% Triton. DAPI was washed away with 0.1% Triton and slides were mounted using Aqua-Poly/Mount.

UDS. Cells were grown to confluency on coverslips and serum-deprived (0.5%) for 2 days to arrest cells in G0. Cells were irradiated with 16 J/m^2 and labelled with 20 µM EdU (Invitrogen) in Ham's F10 supplemented with 10% dialysed FCS and 20 mM HEPES buffer (both Gibco) for 3 h before fixation for 15 min (3.7% FA and 0.5% Triton X-100). The background signal was blocked by washing twice with 3% BSA in PBS for 10 min, and nuclei were permeabilized for 20 min using 0.5% Triton in PBS. EdU incorporation was visualized using Click-it chemistry, imaged and analysed as described in the section "EU incorporation" with the adjustment that the Click-it reaction was performed for 30 min.

Yeast strains. Yeast deletion strains used in this study are derivatives of the WT strain BY4741 (*MATa his3Δ1 leu2Δ0 met15Δ0 ura3Δ0*) and Y452 (*MATα, ura3-52, his3–1, leu2-3, leu2-112, cir°*). The gene deletions were made by transforming the yeast cells with PCR products bracketing selection markers[59] or by following published methods[60].

Yeast UV sensitivity assay. Yeast cells were grown in YPD medium to mid-log phase. For the spotting assay, cells were serially diluted tenfold in fresh YPD medium and spotted on YPD plates. After exposure to different doses of UV-C light (254 nm), plates were incubated at 30 °C in the dark and images were taken after 3–5 days of incubation. For the quantitative UV survival assay, diluted yeast cells were plated on YPD plates and exposed to the indicated UV doses. The number of colonies on each plate was counted after incubating for 3 days at 30 °C in the dark.

CPD-seq library preparation and sequencing. CPD-seq analysis of repair in WT and *elf1*Δ mutant strains was performed as previously described[33]. Briefly, yeast cells were grown to mid-log phase, pelleted, re-suspended in distilled H_2O (dH_2O) and irradiated with 125 J/m^2 UV-C light (254 nm). After UV treatment, cells were incubated in the dark in pre-warmed, fresh YPD medium for repair. Cells were collected before UV irradiation (no UV), immediately after UV (0 h) and following a 2-h repair incubation. The cells were pelleted and stored at −80 °C until genomic DNA isolation.

Genomic DNA extraction, CPD-seq library preparation and quality control, sequencing with an Ion Proton sequencer and data processing were all performed as previously described[33]. The resulting sequencing reads were aligned to the yeast genome (saccer3) using Bowtie 2 (ref. [61]). Only CPD-seq reads associated with lesions at dipyrimidine sequences (that is, TT, TC, CT and CC) were retained for further analysis.

Bin analysis for CPD repair along the TS and NTS of ~5,000 yeast genes was performed as previously described[62] using TSS and polyadenylation site (PAS, also referred to as transcription termination site (TTS)) coordinates from Park et al.[63]. A similar gene bin analysis is displayed for each yeast gene using the Java Treeview program[64,65]. Genes were sorted according to the transcription rate, which was obtained from a published gene-expression database of transcription frequencies for WT yeast[66]. Single-nucleotide resolution repair analysis adjacent to the TSS was performed as previously described[62,67]. Nucleosome dyad coverage from MNase-seq experiments were obtained from Weiner et al.[51] as reference. CPD-seq data for *elf1*Δ and WT yeast were normalized using the fraction of CPDs remaining determined for bulk genomic DNA by T4 endonuclease V digestion and alkaline gel electrophoresis (see below).

Analysis of bulk CPD repair in UV-irradiated yeast. Alkaline gel electrophoresis to assay global DNA repair of bulk DNA was conducted as previously described[68]. Yeast cell cultures were grown to mid-log phase in YPD media. Yeast cell cultures were briefly centrifuged to pellet, resuspended in dH_2O and exposed to 100 J/m^2 UV-C light or left unirradiated for the 'no UV' sample. Following irradiation, yeast cells were resuspended in YPD and incubated at 30 °C. Aliquots were taken at each repair time point, briefly centrifuging to discard medium supernatant before storing yeast cells at −80 °C. Genomic DNA was isolated by bead beating the yeast cell pellets in 250 µl lysis buffer (2% Triton-X 100, 1% SDS, 100 mM NaCl, 10 mM Tris-Cl pH 8 and 1 mM Na_2EDTA) and 300 µl phenol–chloroform-isoamyl alcohol (25:24:1). TE pH 8 buffer (300 µl) was added to each tube, briefly vortexing to mix. Samples were centrifuged and the DNA-containing aqueous layer was transferred to a fresh tube for ethanol precipitation. DNA pellets were resuspended in TE pH 8 containing 0.2 mg ml^{-1} RNase A, incubating at 37 °C for 15 min before enzymatic digestion. Equal amounts of DNA were then treated with T4 endonuclease V (T4 PDG; NEB) and resolved by electrophoresis on a 1.2% alkaline agarose gel. Following neutralization and staining with SYBR Gold (Invitrogen), alkaline gels were imaged using a Typhoon FLA 7000 (GE Healthcare) and analysed using ImageQuant TL 8.2 (GE Healthcare). The number of CPD lesions per kb was estimated using the ensemble average pixel density of each lane, corrected by the no enzyme control lane. The percent repair was calculated by normalizing the number of CPDs per kb to the no repair time point. Graphs represent the mean and s.e.m. of at least three independent experiments.

Repair analysis of UV-induced CPDs in the *RPB2* locus. Yeast cells were grown in synthetic dextrose medium at 30 °C to late-log phase ($A_{600} \approx 1.0$), irradiated with 120 J/m^2 of UV-C and incubated in YPD medium at 30 °C in the dark. At different times of the repair incubation, aliquots were removed and the genomic DNA was isolated. To map the induction and repair of UV-induced CPDs at the nucleotide

resolution in a specific gene, libraries of DNA fragments adjoining the lesions were created by using the lesion-adjoining fragment sequencing strategy[69] with some modifications. Briefly, the isolated genomic DNA was restricted with HincII and NruI to release a 553-bp *RPB2* gene fragment (168-bp upstream and 385-bp downstream of the TSS) and incised at the CPDs with T4 endonuclease V and treated *Escherichia coli* endonuclease IV (New England Biolabs). The 3′ ends of the restricted and CPD-incised DNA fragments were ligated to Illumina sequencing adapters using Circligase (Lucigen). After PCR amplification, the libraries were sequenced using an Illumina HiSeq platform.

The sequencing reads were aligned to the *RPB2* gene using Bowtie 2 (ref. [61]). The numbers of reads from the UV-irradiated samples were normalized to those from the control (non-irradiated) samples. Reads corresponding to CPDs at individual sites along the *RPB2* gene fragment were counted after subtraction of the background counts (in the non-irradiated samples) by using codes in R. To more directly 'visualize' the CPD induction and repair profiles, images with band intensities corresponding to counts of aligned sequencing reads were created using codes in R and Matlab.

***C. elegans* strains and UV-sensitivity assays.** *C. elegans* strains were cultured according to standard methods and outcrossed against Bristol N2, which was used as the WT. Mutant alleles were *xpc-1(tm3886)*, *csb-1(ok2335)* and *elof-1(emc203)*. The loss-of-function *elof-1(emc203)* (Extended Data Fig. 6i) mutant strain was generated by injection of Cas9 protein together with tracrRNA and two crRNAs targeting *elof-1* (CAGTTGAATTGGGTGTCGAG and AGACGTCGATTGGCTCGGAG; Integrated DNA Technologies). Deletion animals were selected by genotyping PCR and sequencing. UV survival experiments were performed as previously described[36]. Animals were irradiated at the indicated dose using two Philips TL-12 (40 W) tubes emitting UV-B light. Briefly, germ cell and embryo UV survival was determined by allowing UV-irradiated staged young adults to lay eggs on plates for 3 h. To calculate the survival percentage, the total number of hatched and unhatched eggs was counted after 24 h. For the L1 larvae UV survival experiment, staged L1 larvae were UV irradiated and grown for 48 h. The survival percentage was calculated by counting surviving animals that developed beyond the L2 stage and arrested animals as L1/L2 larvae.

Metaphase spreads and chromosomal aberrations. Metaphase spreads were carried out as previously described[70]. Briefly, cells were irradiated with 4 J/m^2 or mock-treated 48 or 72 h before preparing metaphase spreads (final confluence of 50–80%). Cells were arrested at metaphase by incubating with colcemid (*N*-methyl-*N*-deacetyl-colchicine, Roche, 10295892001) for the last 14 h before collecting the cells. Collected cells were treated with hypotonic solution (0.075 M KCl) for 30 min at 37 °C and fixed with methanol:acetic acid (3:1). Telomere-FISH was further carried out to study chromosomal aberrations. Metaphases were hybridized with telomere-repeat specific peptide nucleic acid probes (Applied Biosystems) as described to label telomeres[71]. A minimum of 60 metaphase images were obtained using a Carl Zeiss Axio Imager D2 microscope with a ×63 Plan Apo 1.4 NA oil-immersion objective and analysed with ImageJ software for chromosomal aberrations.

DNA fibre analysis. DNA fibre analysis was carried out as previously described[70,72]. Briefly, cells were sequentially pulse-labelled with 30 µM CldU (c6891, Sigma-Aldrich) and 250 µM IdU (I0050000, European Pharmacopoeia) for 15 min. For assessing fork progression after DNA damage, cells were irradiated with 4 J/m^2 UV and incubated for 2 h before pulse-labelling. After labelling, cells were collected and resuspended in PBS at 2.5 × 10^5 cells per ml. The labelled cells were mixed 1:1 with unlabelled cells, and 2.5 µl of cells was added to 7.5 µl of lysis buffer (200 mM Tris-HCl, pH 7.5, 50 mM EDTA and 0.5% (w/v) SDS) on a glass slide. After 8 min, the slides were tilted at 15–45°, and the resulting DNA spreads were air dried, fixed in 3:1 methanol/acetic acid overnight at 4 °C. The fibres were denatured with 2.5 M HCl for 1 h, washed with PBS and blocked with 0.2% Tween-20 in 1% BSA/PBS for 40 min. The newly replicated CldU and IdU tracks were incubated (for 2.5 h in the dark, at room temperature with anti-BrdU antibodies recognizing CldU and IdU (Supplementary Table 3)), followed by a 1-h incubation with secondary antibodies at room temperature in the dark (anti-mouse Alexa Fluor 488 and anti-rat Cy3 (Supplementary Table 3)). Fibres were visualized and imaged using a Carl Zeiss Axio Imager D2 microscope with a ×63 Plan Apo 1.4 NA oil-immersion objective. Data analysis was carried out with ImageJ software. A one-way analysis of variance (ANOVA) was applied for statistical analysis using GraphPad Prism software.

Immunofluorescence. Immunofluorescence was carried out as previously described[73]. Cells were grown on 24-mm glass coverslips and mock-treated or irradiated with 8 J/m^2 48, 24 or 6 h before fixation for 15 min in PBS with 3.7% FA. Subsequently, cells were permeabilized with 0.1% Triton X-100 in PBS and washed with PBS+ (0.15% BSA and 0.15% glycine in PBS). Cells were incubated for 2 h at room temperature with rabbit anti-53BP1 antibody (Supplementary Table 3) in PBS+. Thereafter, cells were washed with PBS+, 0.1% Triton and PBS+ before incubating for 2 h at room temperature with donkey anti-rabbit Alexa Fluor 594 conjugated antibody (Supplementary Table 3) and DAPI. After washes with PBS+ and 0.1% Triton, coverslips were mounted with Aqua-Poly/Mount. Images were acquired with a Zeiss LSM700 Axio Imager Z2 upright microscope equipped with a ×63 Plan-apochromat 1.4 NA oil-immersion lens (Carl Zeiss Micro Imaging). The number of foci per nucleus was counted using ImageJ.

Mitotic FANCD2 and EdU foci. HCT116 or RPE-1 *TP53*$^{-/-}$ cells were seeded on glass coverslips in 6-well plates. If indicated, RPE-1 *TP53*$^{-/-}$ cells were transfected with siRNAs for 24 h, after which the cells were irradiated with 4 J/m^2 UV 254 nm using a Stratalinker (Stratagene) and left for 48 h. RPE-1 *TP53*$^{-/-}$ cells were synchronized at the G2/M border using a 4-h incubation with the CDK1 inhibitor RO-3306 (final concentration 5 µM, Axon Medchem, 1530) and released into pro/prometaphase while pulsed with EdU (20 µM) for 30 min. HCT116 cells were irradiated with 4 J/m^2 UV at 24 h after seeding and were left for 48 h. When indicated, cells were pulsed for 30 min with 20 µM EdU. Cells were fixed using 2% FA with 0.1% Triton-X-100 in PBS for 30 min, and were subsequently permeabilized for 10 min in PBS with 0.5% Triton X-100. Cells were than stained with anti-FANCD2 (Novusbio, NB100-182) and Alexa 488 or Alexa 647 conjugated secondary antibodies and counterstained with DAPI (Sigma). The EdU Click-chemistry reaction was performed as per the manufacturer's instructions (Click-iT EdU Cell Proliferation kit for imaging, Alexa Fluor 647, ThermoFisher Scientific).

Statistics and reproducibility. Experimental data were plotted and analysed using GraphPad Prism 9.0.1 (GraphPad Software) built-in tests and are indicated in the figure legends, unless otherwise indicated. The number of samples analysed per experiment are reported in the respective figure legends. All experiments were independently repeated at least two times with similar results obtained.

Reporting Summary. Further information on research design is available in the Nature Research Reporting Summary linked to this article.

Data availability

All the DRB/TT$_{chem}$-seq data used in this study are available under GEO accession number GSE148844. All the CPD-seq data are available under GEO accession number GSE149082. The SILAC-based quantitative interaction proteomics data have been deposited to the ProteomeXchange Consortium via the PRIDE partner repository with the dataset identifier PXD025304. Source data are provided with this paper. Any other data are available from the corresponding author upon reasonable request.

References

52. Campeau, E. et al. A versatile viral system for expression and depletion of proteins in mammalian cells. *PLoS ONE* **4**, e6529 (2009).
53. Yesbolatova, A., Natsume, T., Hayashi, K.-I. & Kanemaki, M. T. Generation of conditional auxin-inducible degron (AID) cells and tight control of degron-fused proteins using the degradation inhibitor auxinole. *Methods* **164–165**, 73–80 (2019).
54. Natsume, T., Kiyomitsu, T., Saga, Y. & Kanemaki, M. T. Rapid protein depletion in human cells by auxin-inducible degron tagging with short homology donors. *Cell Rep.* **15**, 210–218 (2016).
55. Brinkman, E. K., Chen, T., Amendola, M. & van Steensel, B. Easy quantitative assessment of genome editing by sequence trace decomposition. *Nucleic Acids Res.* **42**, e168 (2014).
56. Shalem, O. et al. Genome-scale CRISPR–Cas9 knockout screening in human cells. *Science* **343**, 84–87 (2014).
57. Livak, K. J. & Schmittgen, T. D. Analysis of relative gene expression data using real-time quantitative PCR and the $2^{-\Delta\Delta ct}$ method. *Methods* **25**, 402–408 (2001).
58. Ramirez, F. et al. deepTools2: a next generation web server for deep-sequencing data analysis. *Nucleic Acids Res.* **44**, W160–W165 (2016).
59. Gardner, J. M. & Jaspersen, S. L. Manipulating the yeast genome: deletion, mutation, and tagging by PCR. *Methods Mol. Biol.* **1205**, 45–78 (2014).
60. Brachmann, C. B. et al. Designer deletion strains derived from *Saccharomyces cerevisiae* S288C: a useful set of strains and plasmids for PCR-mediated gene disruption and other applications. *Yeast* **14**, 115–132 (1998).
61. Langmead, B. & Salzberg, S. L. Fast gapped-read alignment with Bowtie 2. *Nat. Methods* **9**, 357–359 (2012).
62. Mao, P., Smerdon, M. J., Roberts, S. A. & Wyrick, J. J. Asymmetric repair of UV damage in nucleosomes imposes a DNA strand polarity on somatic mutations in skin cancer. *Genome Res.* **30**, 12–21 (2020).
63. Park, D., Morris, A. R., Battenhouse, A. & Iyer, V. R. Simultaneous mapping of transcript ends at single-nucleotide resolution and identification of widespread promoter-associated non-coding RNA governed by TATA elements. *Nucleic Acids Res.* **42**, 3736–3749 (2014).
64. Eisen, M. B., Spellman, P. T., Brown, P. O. & Botstein, D. Cluster analysis and display of genome-wide expression patterns. *Proc. Natl Acad. Sci. USA* **95**, 14863–14868 (1998).
65. Saldanha, A. J. Java Treeview—extensible visualization of microarray data. *Bioinformatics* **20**, 3246–3248 (2004).

66. Holstege, F. C. et al. Dissecting the regulatory circuitry of a eukaryotic genome. *Cell* **95**, 717–728 (1998).
67. Mao, P. et al. Genome-wide maps of alkylation damage, repair, and mutagenesis in yeast reveal mechanisms of mutational heterogeneity. *Genome Res.* **27**, 1674–1684 (2017).
68. Hodges, A. J., Plummer, D. A. & Wyrick, J. J. NuA4 acetyltransferase is required for efficient nucleotide excision repair in yeast. *DNA Repair (Amst.)* **73**, 91–98 (2019).
69. Li, M., Ko, T. & Li, S. High-resolution digital mapping of *N*-methylpurines in human cells reveals modulation of their induction and repair by nearest-neighbor nucleotides. *J. Biol. Chem.* **290**, 23148–23161 (2015).
70. Mukherjee, C. et al. RIF1 promotes replication fork protection and efficient restart to maintain genome stability. *Nat. Commun.* **10**, 3287 (2019).
71. Callen, E. et al. ATM prevents the persistence and propagation of chromosome breaks in lymphocytes. *Cell* **130**, 63–75 (2007).
72. Cornacchia, D. et al. Mouse Rif1 is a key regulator of the replication-timing programme in mammalian cells. *EMBO J.* **31**, 3678–3690 (2012).
73. van Cuijk, L. et al. SUMO and ubiquitin-dependent XPC exchange drives nucleotide excision repair. *Nat. Commun.* **6**, 7499 (2015).

Acknowledgements

We thank the Optical Imaging Center and the Proteomics Center of the Erasmus Medical Center for support with microscopes and mass spectrometry analysis. We thank the Advanced Sequencing Facility of the Francis Crick Institute for technical assistance with DRB/TT$_{chem}$-seq. We acknowledge infrastructural support from the Josephine Nefkens Precision Cancer Treatment Program. This work is part of the Oncode Institute, which is partly financed by the Dutch Cancer Society and was funded by a grant from the Dutch Cancer Society (KWF grant 10506). This work was further funded by the Dutch organization for Scientific Research (NWO-ALW), which awarded a VIDI (864.13.004) and VICI (VI.C.182.025) grant to J.A.M. A.R.C. is supported by the Dutch Cancer Society (KWF grant 11008) and NWO VIDI (193.131). S.L. is funded by the National Science Foundation (MCB-1615550). J.J.W. is funded by the National Institute of Environmental Health Sciences (grants R01ES028698, R21ES029655 and R21ES029302). M.A.T.M.v.V. is funded by a grant from the European Research Council (ERC CoS grant 682421). H.L. is funded by The Netherlands Organization for Scientific Research (project number 711.018.007) and Cancergenomics.nl. W.V. was funded by a grant from the European Research Council (agreement 340988). J.Q.S. was supported by the Francis Crick Institute (which receives funding from Cancer Research UK (FC001166), the UK Medical Research Council (FC001166) and the Wellcome Trust (FC001166)) and by a grant from the European Research Council (agreement 693327).

Author contributions

M.E.G. performed the majority of the experiments and generated the *ELOF1* and *CSB* KO cell lines and the *ELOF1* and *RPB1* KI cell lines. D.Z. generated the *CSB* and *UVSSA* KI cells and performed live-cell imaging experiments and the TCR UDS. K.S., D.A.P., W.G., S.L. and J.J.W. performed and supervised all the *S. cerevisiae* experiments. B.S. and M.E.G. performed the CRISPR–Cas9 screen, and B.E. and R.B. analysed and supervised the screen. C.M., C.L. and A.R.C. performed and supervised the metaphase spread, DNA fibre analysis and 53BP1 cell cycle analysis. S.C., R.M. and J.Q.S. performed and supervised the DRB/TT$_{chem}$-seq. M.v.T. performed the AlamarBlue cell-viability assay. M.v.d.W. and H.L. performed and supervised the *C. elegans* experiments. R.C.J. provided experimental support. Y.P.K. performed the EdU and FANCD2 foci analysis, supervised by M.A.T.M.v.V. J.H.G.L. generated images of the Pol II structure. B.G. performed the Monte-Carlo-based modelling and was supervised by A.B.H. K.B. and J.A.A.D. performed and supervised the mass spectrometry analysis. A.R. performed the UDS experiments and A.F.T. performed FACS sorting, both supervised by W.V. J.A.M. conceived and supervised the project and together with M.E.G. wrote the manuscript with input from all authors.

Competing interests

The authors declare no competing interests.

Additional information

Extended data is available for this paper at https://doi.org/10.1038/s41556-021-00692-z.

Supplementary information The online version contains supplementary material available at https://doi.org/10.1038/s41556-021-00692-z.

Correspondence and requests for materials should be addressed to J.A.M.

Peer review Information *Nature Cell Biology* thanks the anonymous reviewers for their contribution to the peer review of this work.

Reprints and permissions information is available at www.nature.com/reprints.

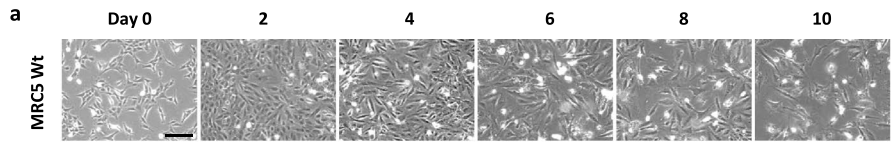

b

GO biological processes. Top 10 terms of n=49 genes (FDR<0.1)

Pathway description	Gene count	Adjusted p-value
nucleotide-excision repair	13 out of 112	1.41E-15
cellular response to DNA damage stimulus	22 out of 873	3.12E-14
transcription-coupled nucleotide-excision repair	11 out of 73	4.46E-14
DNA repair	18 out of 563	1.12E-12
response to UV	12 out of 140	1.55E-12
response to radiation	15 out of 447	2.61E-10
cellular response to stress	25 out of 2105	3.11E-09
DNA metabolic process	18 out of 943	7.67E-09
response to light stimulus	12 out of 313	2.36E-08
nucleic acid metabolic process	34 out of 5207	3.02E-07

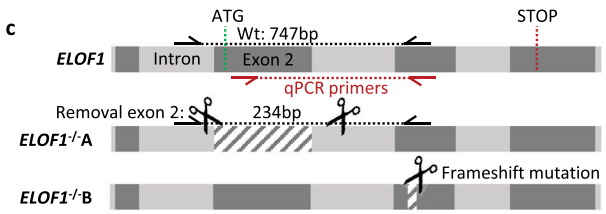

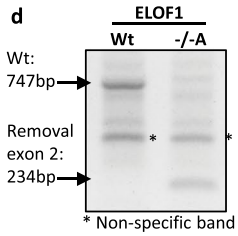

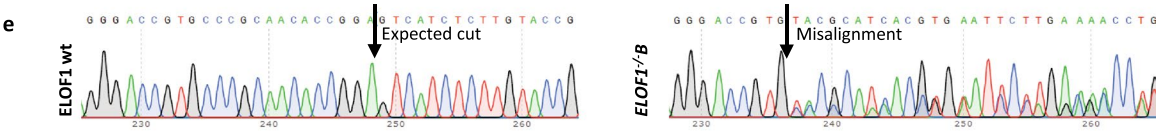

mRNA sequence

Allele 1: 181 GGACCGTG ---------- TA ---------- CCCATAAC 249 25bp + 26bp deletion
Wildtype: 181 GGACCGTGCCCGCAACACCGGAGTCATCTCTTGTACCGTGTGCCTAGAGGAATTCCAGACGCCCATAAC 249
Allele 2: 181 GGACCGTGCCCGCAACACCGGA ---------- ATTCCAGACGCCCATAAC 249 29bp deletion

Amino acid sequence

Allele 1: MGRRKSKRKPPPKKKMTGTLETQFTCPFCNHEKSCDVKMDRVPITCILGNLGFFQRVGRGLESGPCSSGPLCALVQGQSRPEEQVPPSDFCGVRRCRAGFQCQ*
Wildtype: MGRRKSKRKPPPKKKMTGTLETQFTCPFCNHEKSCDVKMDRARNTGVISCTVCLEEFQTPITYLSEPVDVYSDWIDACEAANQ
Allele 2: MGRRKSKRKPPPKKKMTGTLETQFTCPFCNHEKSCDVKMDRARNTGIPDAHNVYPWKPGLFPEGGEGAGVRTLLIWPTVCPGAGPKPSRGTGAT*

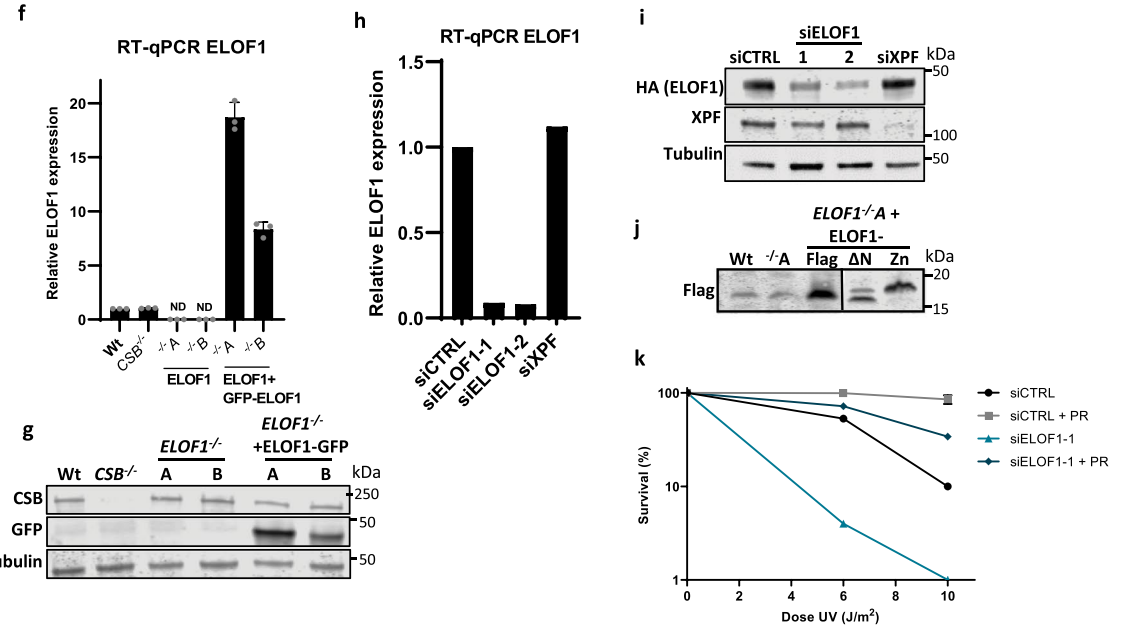

Extended Data Fig. 1 | See next page for caption.

Extended Data Fig. 1 | Generation of ELOF1 knock-in and knock-out cells. a, Brightfield images of MRC-5 cells irradiated with indicated doses of UV-C for 10 consecutive days. Images were taken every other day. Scale bar: 60 µm. **b**, Top 10 enriched GO terms (biological process) identified using g:Profiler of UV-sensitive genes with FDR<0.1 (n = 49). **c**, Schematic of the genomic *ELOF1* locus. Scissors indicate target regions of the sgRNAs used to generated *ELOF1* KO (−/−) cells, half arrows indicate primers used for genotyping as shown in (**c**). Red arrows indicate location of the qPCR primers as shown in (**e**). **d**,**e**, Genotyping of ELOF1 KO (−/−) cells, both originating from a single cell clone. **d**, Genotyping PCR of loss of exon 2 in *ELOF1* −/−A cells. Assays in d, i, j and g have been performed two times with similar results. **e**, Top panel: Sequencing results showing frameshift mutations in the targeted genomic locus of *ELOF1* −/−B. Bottom panel: Amino acid sequence of ELOF1 in ELOF1 −/−B cells. **f**, Relative ELOF1 levels in indicated HCT116 Wt and ELOF1 KO (−/−) cells, with ELOF1 re-expression where indicated, as determined by RT-qPCR. Relative ELOF1 mRNA expression was normalized to GAPDH signal and levels in Wt cells were set to 1. ND=not detected. Data shown in represent average ± SEM (n = 3 independent experiments. **g**, Immunoblot of indicated HCT116 cell lines showing CSB or ELOF1-GFP expression. Tubulin was used as loading control. **h**, Relative ELOF1 levels in HCT116 cells transfected with indicated siRNAs as determined by RT-qPCR. Relative ELOF1 expression was normalized to GAPDH signal and siCTRL levels were set to 1. Data shown represent average from 2 independent experiments. **i**, Immunoblot showing endogenous ELOF1 and XPF levels in *ELOF1-mScarletI-HA* KI cells (Extended Data Fig. 2a) transfected with indicated siRNAs. Tubulin was used as loading control. **j**, Immunoblot showing expression of Flag-tagged Wt or indicated ELOF1 mutants in HCT116 ELOF1 −/−A cells. **k**, Relative colony survival of CPD photolyase cells transfected with indicated siRNAs. PR indicates CPD removal by photoreactivation. Plotted curves represent averages of 2 independent experiments. Numerical data and uncropped blots are provided in source data.

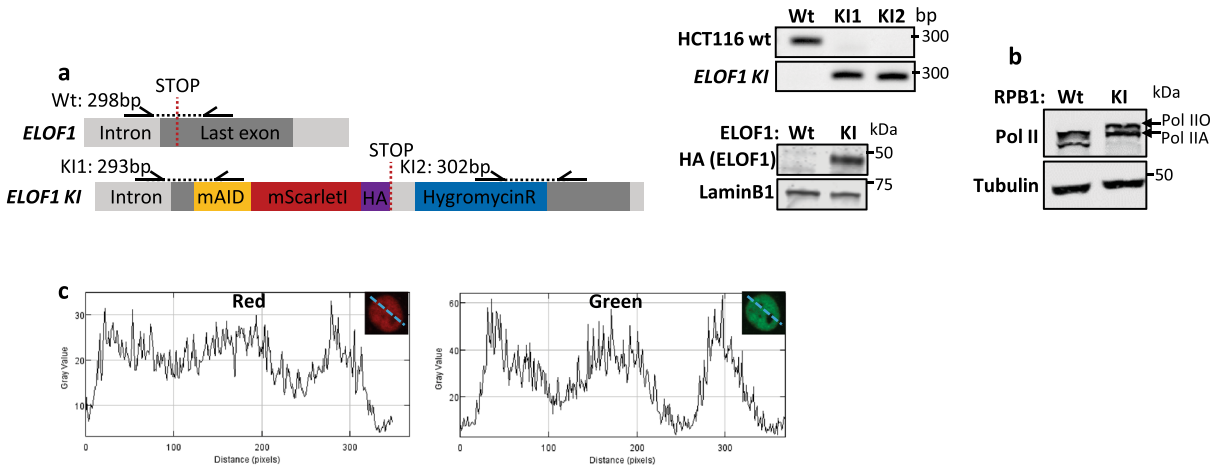

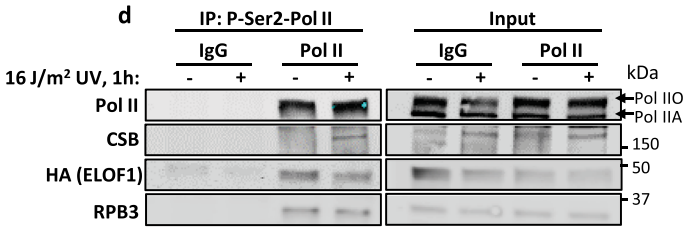

f

GO biological processes. Top 10 terms of n=55 genes (SILAC ratio ≥ 2.5)

Pathway description	Gene count	Adjusted p-value
RNA processing	34 out of 941	2.99E-29
transcription elongation from RNA polymerase II promoter	18 out of 83	3.18E-27
DNA-templated transcription, elongation	18 out of 111	9.67E-25
RNA metabolic process	44 out of 4714	2.68E-17
nucleic acid metabolic process	45 out of 5207	8.10E-17
mRNA processing	21 out of 523	1.67E-16
snRNA transcription by RNA polymerase II	12 out of 71	1.06E-15
snRNA transcription	12 out of 72	1.27E-15
ncRNA transcription	13 out of 108	3.31E-15
gene expression	45 out of 5672	3.34E-15

e

GFP-RPB1 IP
Interactors GFP-RPB1 / Wt

	Gene names	Average SILAC ratio
Pol II	POLR2A	37.17
	POLR2B	19.09
	POLR2C	19.57
	POLR2D	29.05
	POLR2E	8.50
	POLR2G	5.62
	POLR2H	15.68
	POLR2I	8.27
	POLR2J	18.27
	POLR2L	12.70
	ELOF1*	4.98
Elongation factors	IWS1	8.31
	SUPT4H1	4.61
	SUPT5H	11.33
	SUPT5H	8.76
	SUPT6H	14.30
	TCEA1	4.93
	RECQL5	5.23
PAF complex	CDC73	3.83
	CTR9	4.48
	LEO1	4.54
	PAF1	3.65

Extended Data Fig. 2 | See next page for caption.

Extended Data Fig. 2 | ELOF1 is part of the Pol II complex. a, Left panel: Schematic of the genomic locus of *ELOF1* for generating *ELOF1-mScarletI-HA* KI cell line. Half arrows indicate primer locations. Right panel: Genotyping PCR and immunoblot for *ELOF1*-KI cell line (top). LaminB1 was used as loading control (bottom). **b**, Immunoblot of HCT116 *GFP-RPB1* KI. Tubulin was used as loading control. Immunoblots have been performed two times with similar results. **c**, Histograms showing intensities of GFP and mScarletI measured over the indicated dotted line in HCT116 double KI cells. **d**, Native immunoprecipitation of P-Ser2-modified Pol II in HCT116 cells followed by immunoblotting for indicated proteins. Cells were harvested 1 hour after mock treatement or irradiation with 16 J/m^2 UV-C. IgG was used as binding control. IP has been performed two times with similar results. **e**, Interaction heat map based on the SILAC ratios of MRC-5 GFP-RPB1-interacting proteins as determined by quantitative interaction proteomics. Average SILAC ratios of duplicate experiments are plotted and represent RPB1-interactors relative to empty beads. SILAC ratio >1 indicates increase in interaction. * indicates proteins quantified in one experiment. **f**, Top 10 enriched GO terms (biological processes) identified using g:Profiler of 55 proteins identified as ELOF1 interactor with an average SILAC ratio of 2.5 or higher. Uncropped blots are provided in source data.

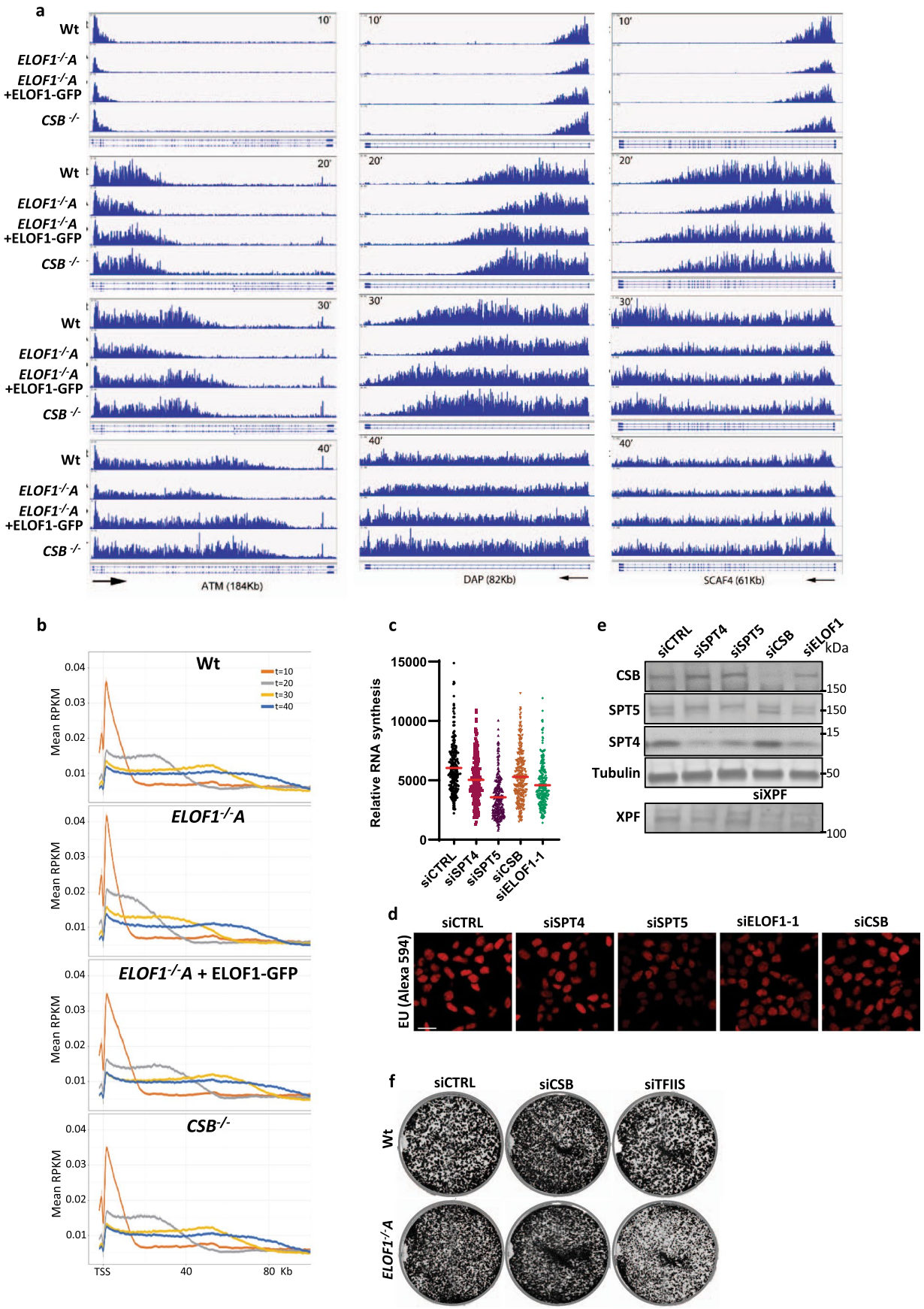

Extended Data Fig. 3 | See next page for caption.

Extended Data Fig. 3 | ELOF1 stimulates transcription elongation. a, Browser tracks from DRB/TT_{chem}-seq experiment at *ATM, DAP* and *SCAF4*. Results are shown 10, 20, 30 or 40 minutes after DRB release. **b**, Metagene profiles of DRB/TT_{chem}-seq in HCT116 Wt or indicated KO (−/−) cells, with ELOF1 re-expression where indicated, 10, 20, 30, or 40 minutes after DRB release for 50-100Kb long genes. **c**, Transcription levels as determined by relative EU incorporation in HCT116 cells transfected with indicated siRNAs. Red lines indicate average integrated density ± SEM. siCTRL n = 247, siSPT4 n = 272, siSPT5 n = 288, siCSB n = 286, siELOF1 #1 n = 285 cells analyzed across 3 (siELOF1 and siCSB) and 4 (siCTRL) independent experiments. **d**, Representative images of EU incorporation in HCT116 cells transfected with indicated siRNAs. Scale bar: 20 μm. **e**, Immunoblot for indicated proteins in HCT116 cells transfected with indicated siRNAs. Tubulin was used as loading control. Experiment has has been performed two times with similar results. **f**, Images of HCT116 Wt and ELOF1 −/−A cells transfected with indicated siRNAs, stained with coomassie blue 10 days after transfection. Cell growth experiment has been executed two times with similar results. Numerical data and uncropped blots are provided in source data.

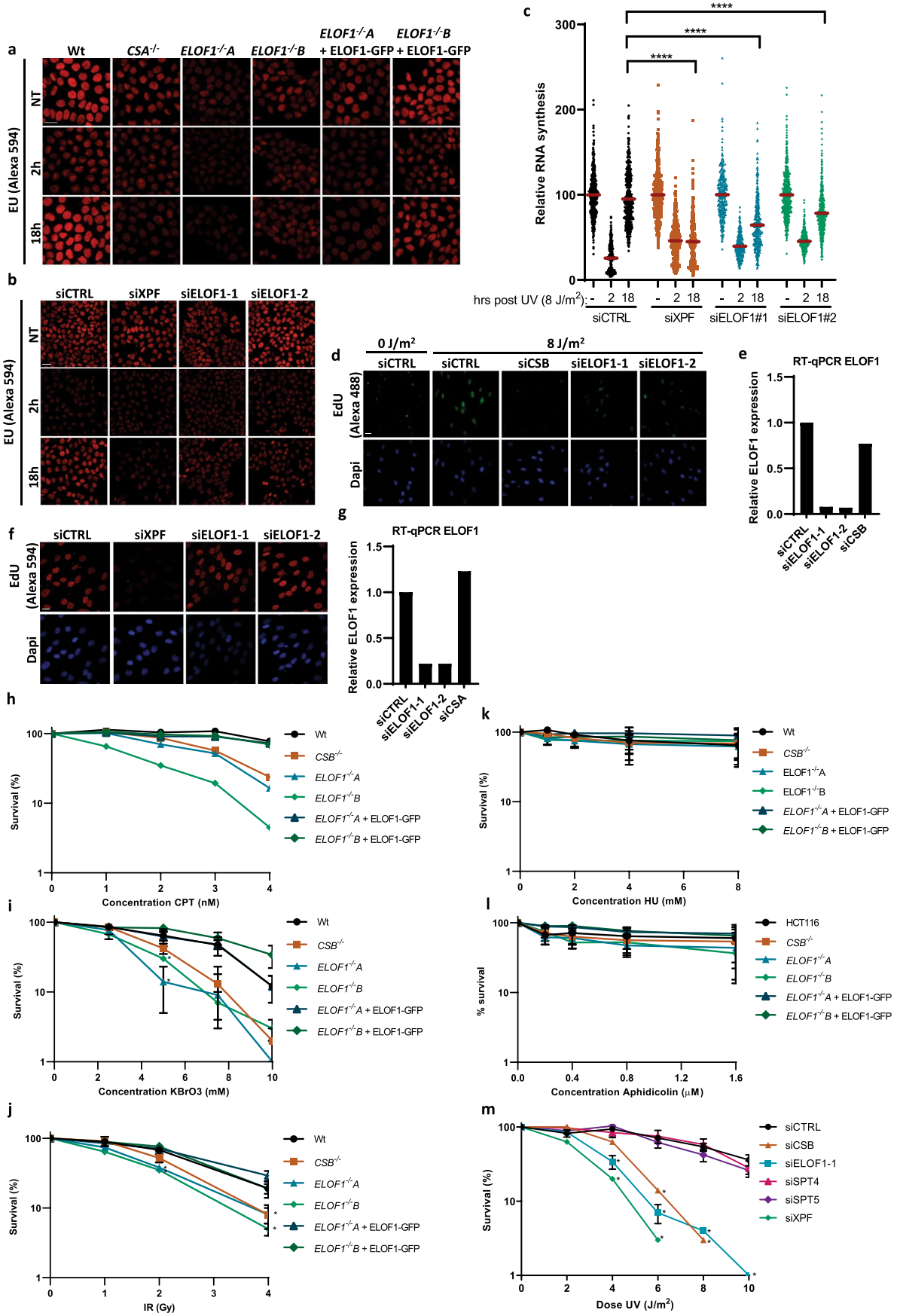

Extended Data Fig. 4 | See next page for caption.

Extended Data Fig. 4 | Role of ELOF1 during TC-NER and protection against different DNA damaging agents. a,**b**, Representative immunofluorescence images of EU incorporation in (**a**) indicated HCT116 cells, or **b**, HCT116 cells transfected with indicated siRNAs, 2 or 18 hours after 8 J/m^2 UV-C or mock treatment (NT). Scale bar: 20 μm. **c**, Transcription restart after UV damage as determined by relative EU incorporation in HCT116 cells transfected with indicated siRNAs, 2 or 18 hours after 8 J/m^2 UV-C or mock treatment (NT). Relative integrated density of UV-irradiated samples are normalized to mock-treated and set to 100%. Red lines indicate average integrated density of, respectively n = 492, 485, 435, 487, 461, 395, 352, 399, 380, 644, 575, 512 cells collected from three independent experiments. **d**, Representative immunofluorescence images of amplified EdU signal in XP186LV fibroblasts (XP-C) transfected with indicated siRNAs, 7 hours after exposure to 8 J/m^2 UV-C. Scale bar: 20 μm. TCR-UDS has been performed three times with similar results. **e**, Relative ELOF1 mRNA levels in XP186LV fibroblasts (XP-C) following transfection with indicated siRNAs determined by RT-qPCR. ELOF1 expression was normalized to GAPDH expression and siCTRL levels were set to 1. Data shown represent average of 2 independent experiments. **f**, Representative fluorescence images of EdU incorporation 3 hours after irradiation with 16 J/m^2 UV-C in C5RO (hTert) cells transfected with indicated siRNAs. Scale bar: 20 μm. (**g**) as in (**f**) in C5RO (hTert) cells. Data shown represent average of 2 independent experiments. **h–k**, Relative colony survival of indicated HCT116 Wt and KO (−/−) cells, with ELOF1 re-expression where indicated, continuously exposed to indicated concentrations of (**h**) camptothecin (CPT) or (**i**) potassium bromate ($KBrO_3$), or irradiated with indicated doses of (**j**) ionizing radiation (IR), or exposed to indicated concentrations of (**k**) hydroxyurea (HU) or (**l**) aphidicolin. Plotted curves represent averages ± SEM. CPT: n = 2; $KBrO_3$: n = 3; IR: n = 5; HU: n = 3, others n = 4 independent experiments. **m**, Relative colony survival of HCT116 cells transfected with indicated siRNAs following exposure to indicated doses of UV-C. Plotted curves represent averages ± SEM. siCTRL, siSPT4 and siSPT5 n = 4, siELOF1 #1, siCSB, siXPF n = 2 independent experiments. *P ≤ 0.05, ****p ≤ 0.0001 analyzed by two-sided unpaired T-test in (**c**) and one-sided unpaired T-test in (**h**-**m**). Numerical data are provided in source data.

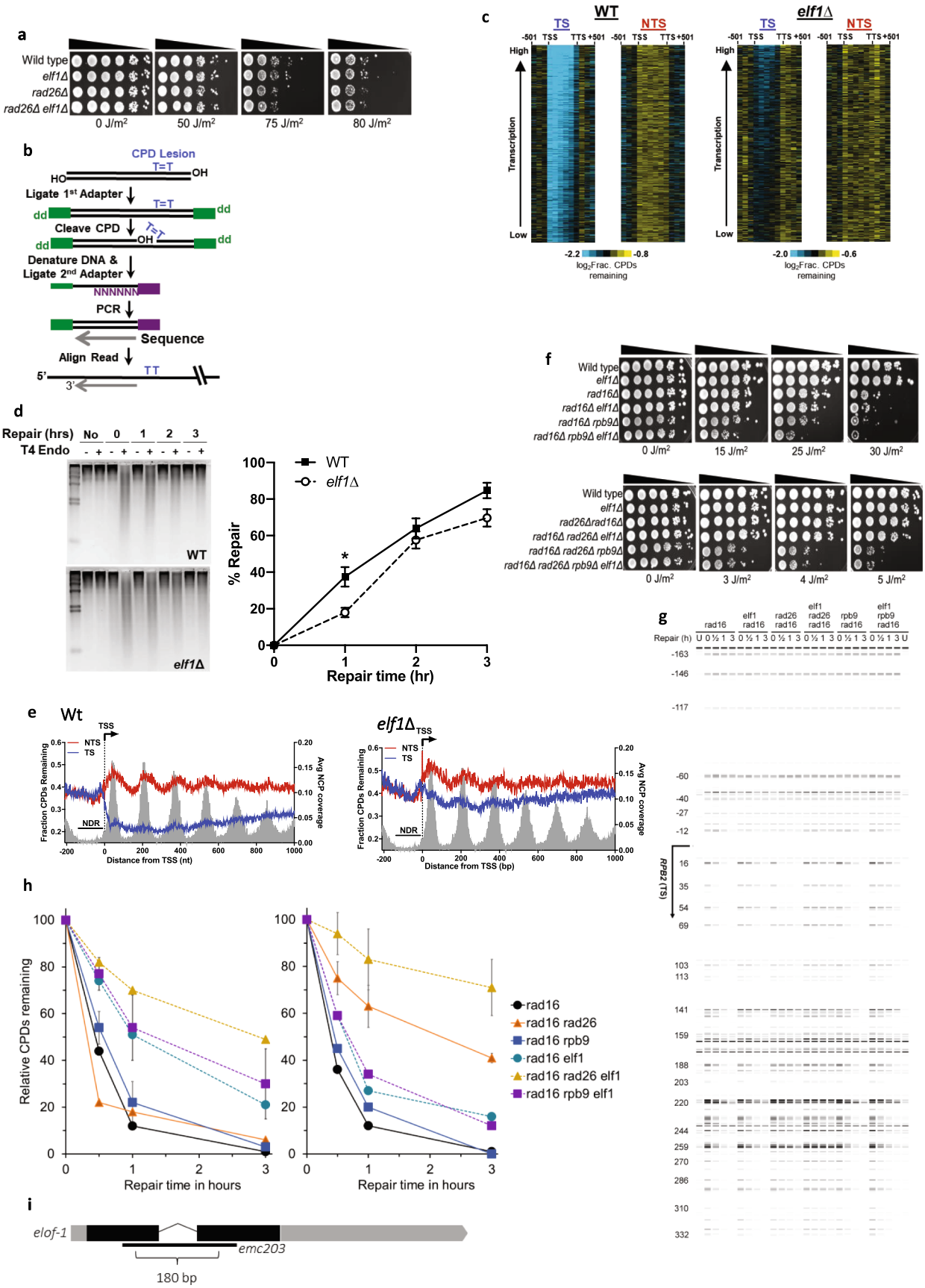

Extended Data Fig. 5 | See next page for caption.

Extended Data Fig. 5 | Role of yeast *elf1* in TC-NER. a, Indicated mutant yeast strains were serially tenfold diluted, spotted, and exposed to indicated UV-C doses. Spot assay has been performed three times with similar results. **b**, Schematic showing the CPD-seq method. Isolated DNA is sonicated and adaptors are ligated. CPDs are cleaved by T4 endonuclease V and APE1 nuclease to generate 3′ ends. Following denaturing of the DNA, ends are ligated to a second adaptor that allows CPD sequencing. **c**, Gene plot analysis of CPD-seq data for ~4500 yeast genes, ordered by transcription frequency[66]. Plots depict unrepaired CPDs following 2-hour repair relative to no repair for both the transcribed strand (TS) and non-transcribed strand (NTS). Each row represents approximately 10 genes. TSS=transcription start site, TTS=transcription termination site. **d**, Left panel: Representative gel of bulk repair of UV-induced CPD lesions in Wt and *elf1*Δ mutant yeast measured by T4 endonuclease V digestion and alkaline gel electrophoresis of genomic DNA isolated from UV-irradiated yeast (100 J/m^2 UV-C light) after the indicated time. Right panel: Quantification of CPD repair from n = 3 WT and n = 4 elf1Δ experiments ±SEM. *$P \leq 0.05$ analyzed by unpaired two-sided t-test. **e**, Single nucleotide resolution analysis of CPD-seq data downstream of the TSS of ~5200 yeast genes. Plots depict fraction of unrepaired CPDs following 2-hour repair relative to no repair for both TS and NTS. Nucleosome positioning data[51] is shown for reference. **f**, Controls for UV spotting assays shown in Fig. 4d. **g**, Image showing repair of CPDs in the TS of the *RPB2* gene for indicated yeast strains. The image was generated by converting sequencing reads aligned to RPB2 into bands. *U:* unirradiated cells. Nucleotide positions relative to TSS (+1) are indicated on the left. **h**, Left: Relative percentage of CPDs remaining within 54 bp downstream of the TSS of the *RPB2* gene. Right: Relative percentage of CPDs remaining in the downstream region (69-353 bp) of the *RPB2* gene. Data are presented as mean values from all CPD sites within the indicated regions (0-54 and 69-353 bp) of the RPB2 gene ±SD from one single experiment, error bars are shown for most relevant strains. n = 8 sites (left panel), and n = 73 (right panel). **i**, Representation of the *C. elegans elof-1* genomic organization, depicting the 180 bp *emc203* deletion allele generated with CRISPR-Cas9. Shaded boxes: exons, black: coding sequences. Numerical data are provided in source data .

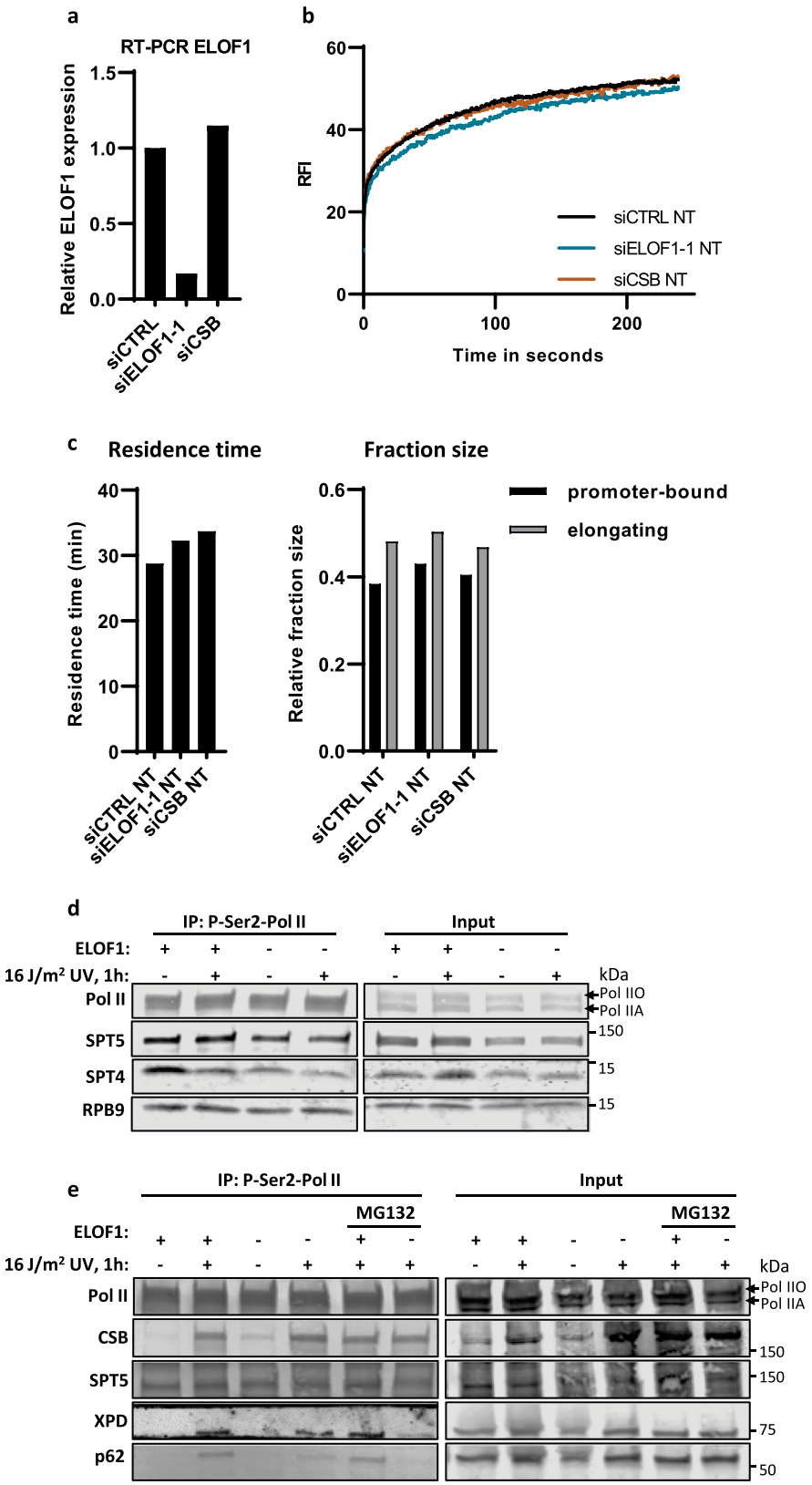

Extended Data Fig. 6 | See next page for caption.

Extended Data Fig. 6 | Effects of ELOF1 deficiency on Pol II elongation speed and complex composition. a, Relative ELOF1 mRNA levels in *GFP-RPB1* KI cells transfected with indicated siRNAs as determined by RT-qPCR. ELOF1 expression was normalized to GAPDH signal and levels of control cells were set to 1. Data shown represent average of 2 independent experiments. **b**, FRAP analysis of GFP-RPB1 mobility after depletion of indicated factors. Mock-treated curves corresponding to Fig. 4a. siCTRL n = 28, siELOF1 #1 n = 20, siCSB NT n = 14 cells analyzed across 4, 3 and 3 independent experiments respectively. **c**, Left panel: Residence time of elongating Pol II or right panel: relative fraction size of promoter-bound or elongating Pol II as determined by Monte-Carlo-based modeling of RPB1 mobility as shown in (**a**). **d**, Native immunoprecipitation of Pol II in Wt and ELOF −/−A cells followed by immunoblotting for indicated proteins. Cells were harvested 1 hour after mock treatment or irradiation with 16 J/m^2 UV-C. MG132: treatment with 50 μM proteasome inhibitor MG132, 1 hour before UV irradiation. **e**, Native immunoprecipitation of Pol II in Wt and ELOF −/−A cells followed by immunoblotting for indicated proteins. Cells were harvested 1 hour after mock treatment or irradiation with 16 J/m^2 UV-C. IP experiments depicted in d and e were executed two times with similar results. Numerical data and uncropped blots are provided in source data.

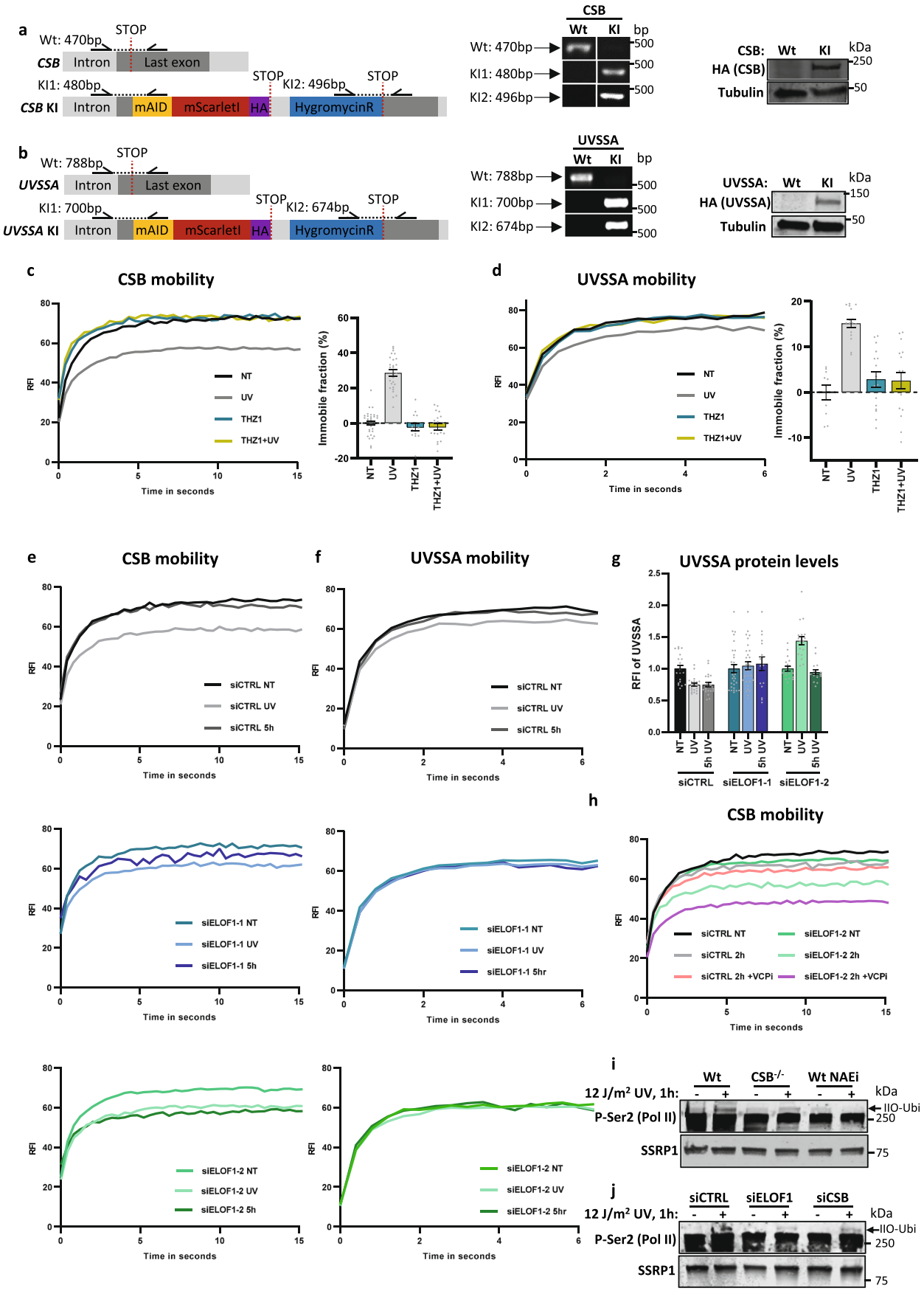

Extended Data Fig. 7 | See next page for caption.

Extended Data Fig. 7 | ELOF1 KO impairs recruitment of UVSSA but not CSB. a, Left panel: Schematic of the genomic locus of *CSB* and used strategy for generating the homozygous *CSB-mScarletI-HA* KI cell line. Half arrows indicate primer locations. Middle and right panel: Genotyping PCR and immunoblot for *CSB*-KI cell line. **b**, Left panel: Schematic of the genomic locus of *UVSSA* and used strategy for generating the homozygous *UVSSA- mScarletI-HA* KI cell line. Half arrows indicate primer locations. Middle and right panel: Genotyping PCR and immunoblot for *UVSSA*-KI cell line. Experiments depicted in a and b were performed two times with similar results. **c**, Left panel: CSB mobility was determined by FRAP analysis of CSB-mScarletI after the indicated treatments. THZ1: 1 hour treatment (2 μM) before UV-C irradiation (4 J/m^2) or mock treatment. Right panel: Relative immobile fraction of CSB as determined by FRAP analysis. Plotted values represent mean ± SEM and are normalized to mock treated. NT n = 32; UV n = 28; THZ1 n = 15; THZ1+UV n = 18 cells analyzed across 2 independent experiments. **d**, Same as C but for UVSSA-mScarletI. NT n = 10; UV n = 16; THZ1 n = 16; THZ1+UV n = 17 cells analyzed across 2 independent experiments. **e**,**f**, FRAP analyses of CSB-mScarletI (**e**) or UVSSA-mScarletI (**f**) mobility after transfection with indicated siRNAs in individual graphs. Cells were mock treated (NT) or analyzed directly (UV) or 5 hours (5hr UV) after irradiation with 4 J/m^2 UV-C. **g**, Relative fluorescence intensity of UVSSA in *UVSSA*-KI cells transfected with indicated siRNAs as determined by live-cell imaging. Plotted values represent mean ± SEM. siCTRL NT n = 30, UV+5h UV n = 21; siELOF1 #1 NT n = 38, UV n = 34, 5h UV n = 16; siELOF1 #2 NT+UV n = 19, 5h UV n = 16 cells analyzed across 4 independent experiments for siCTRL and 3 for siELOF1 and siCSB. **h**, FRAP analysis of CSB in *CSB*-KI cells transfected with indicated siRNAs 2 hours after UV. VCPi: VCP inhibitor (5 μM) was directly added after UV-C (4 J/m^2). **i**, Immunoblot of chromatin fraction of indicated cell lines 1 hour after 12 J/m^2 UV-C or mock treatment. NAEi = 1 hour treatment with NEDDylation inhibitor (10 μM). SSRP1 is shown as loading control. **j**, Immunoblot of chromatin fraction of HCT116 cells transfected with indicated siRNAs 1 hour after 12 J/m^2 UV-C or mock treatment. SSRP1 is shown as loading control. Immunoblots depicted in i and j were executed two times with similar results. Numerical data and uncropped blots are provided in source data.

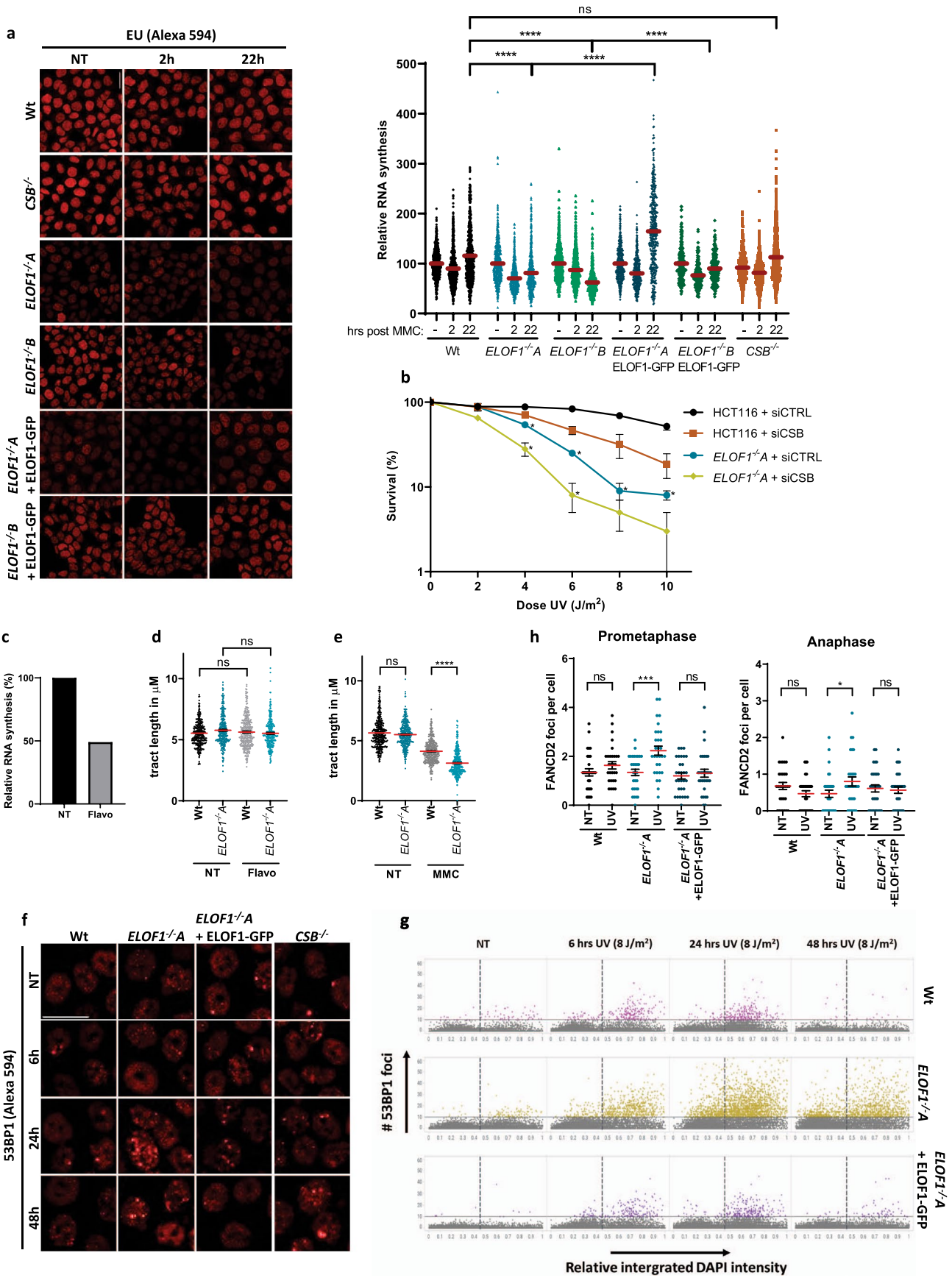

Extended Data Fig. 8 | See next page for caption.

Extended Data Fig. 8 | The additional role of ELOF1 in preventing transcription-mediated replication hindrance. a, Left panel: Representative immunofluorescence images of EU incorporation in indicated HCT116 cells, untreated, or 2 or 22 hours after a 2-hour exposure to 10 μg/ml mitomycin C. Scale bar: 20 μm. Right panel: Transcription restart after mitomycin C as determined by relative EU incorporation in the indicated HCT116 cells. Mitomycin C-treated samples are normalized to mock treated levels and set to 100%. Red lines indicate average integrated density ± SEM of, respectively, n = 1008, 1008, 727, 938, 960, 715, 1133, 1162, 784, 884, 616, 461, 978, 1013, 693, 221, 220, 206 cells collected from four independent experiments. **b**, Relative colony survival of indicated cell lines with siRNA transfection following exposure to indicated doses of UV-C. Plotted curves represent averages ± SEM, n = 3 independent experiments. **c**, Percentage of RNA synthesis in untreated HCT116 cells and cells treated with 0.1 μM flavopiridol for 2 hours as determined by FACS-based quantification of EU pulse labeling. Experiment has been performed two times with similar results. **d**, Fork progression measured by tract lengths of CldU (red) in μm is depicted for indicated HCT116 cells, untreated or after 15 minutes 0.1 μM flavopiridol treatment. Tracts of respectively n = 300, 300, 304 cells collected from two independent experiments. **e**, As (**d**) but after treatment for 1 hour with 25 nM MMC. Tracts of, respectively n = 406, 422, 408, 406 cells collected from two independent experiments. **f**, Representative immunofluorescence images of 53BP1 foci in indicated HCT116 cells, untreated or 6, 24 or 48 hours after exposure to 8 J/m^2 UV-C. Scale bar: 20 μm. **g**, Number of 53BP1 foci as determined in (**f**) quantified by Cellprofiler and plotted against normalized integrated intensity of DAPI, respectively, n = 10494, 7870, 13916, 16647, 9539, 8313, 8610, 8817, 11253, 10950, 10314, 10494 cells collected from two independent experiments. **h**, Number of FANCD2 foci per mitosis in prometaphase (left) or anaphase (right) in indicated HCT116 cells in untreated conditions or 48 hours after 4J/m^2 UV-C. n = 90 cells collected from 3 independent experiments for all conditions. *$p \leq 0.05$, ***$p \leq 0.001$, ****$p \leq 0.0001$ analyzed by two-sided unpaired T-test (**a**), one-sided unpaired T-test (**b**), Kruskal-Wallis test for multiple comparisons (d,e), and two-sided unpaired t-test (Mann-Whitney) (**h**). Numerical data are provided in source data.

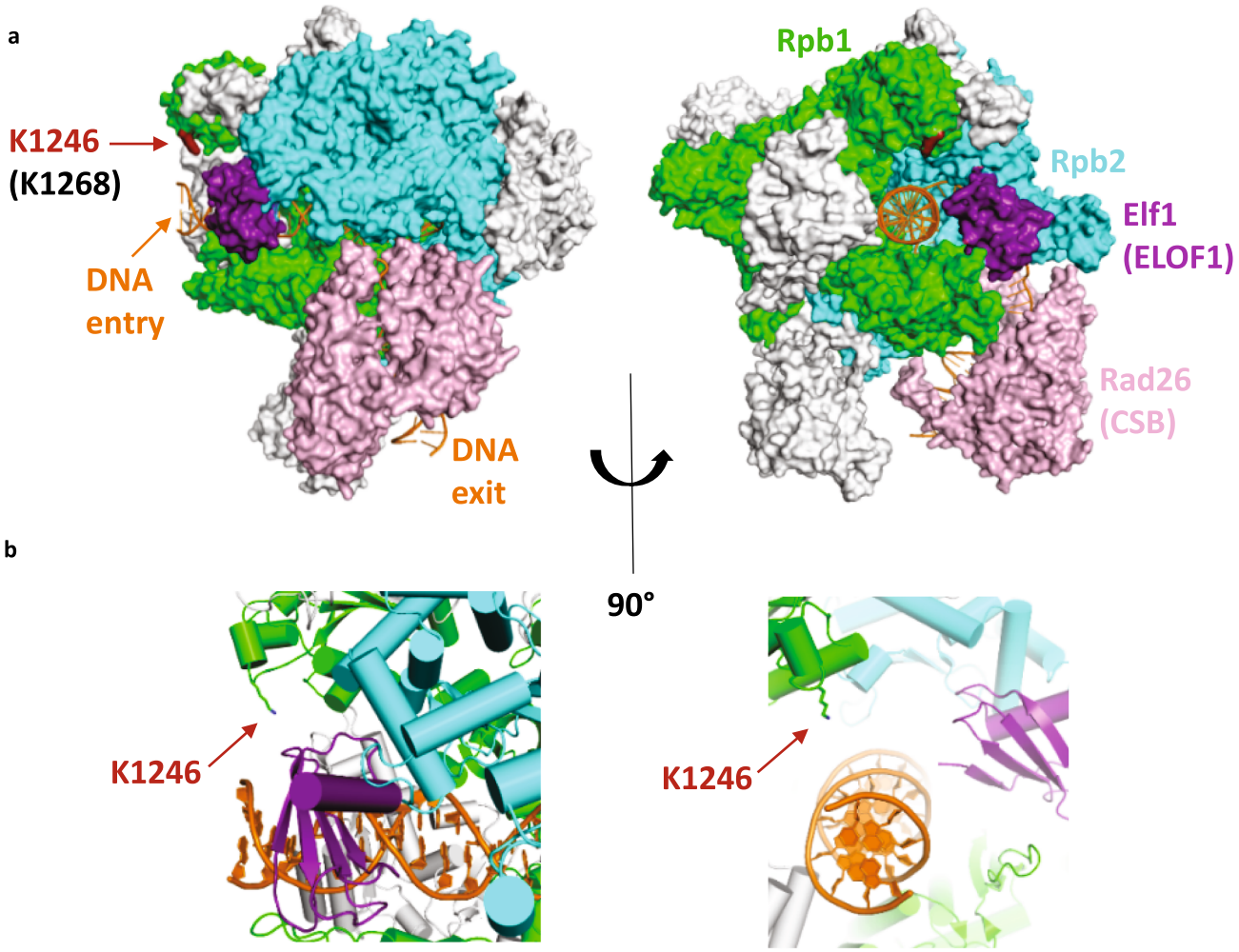

Extended Data Fig. 9 | Pol II-ELOF1 complex structure together with CSB. a, *S.cerevisiae* Pol II (5vvr.pdb) with Rpb1 in green, Rpb2 in cyan, DNA in orange and Rad26 (CSB) in pink. The *P.pastoris* Pol II in complex with elongation factors (5xog.pdb) was superimposed onto this structure (Rpb1 subunits aligned onto each other), and all subunits except Elf1 (ELOF1; purple) were omitted for clarity. Conserved lysine K1246 (K1268 in mammalian Pol II) is indicated in dark red. **b**, Close up of Elf1 (ELOF1) binding region.

nature research

Corresponding author(s): Marteijn

Last updated by author(s): Apr 9, 2021

Reporting Summary

Nature Research wishes to improve the reproducibility of the work that we publish. This form provides structure for consistency and transparency in reporting. For further information on Nature Research policies, see our Editorial Policies and the Editorial Policy Checklist.

Statistics

For all statistical analyses, confirm that the following items are present in the figure legend, table legend, main text, or Methods section.

n/a	Confirmed	
☐	☒	The exact sample size (*n*) for each experimental group/condition, given as a discrete number and unit of measurement
☐	☒	A statement on whether measurements were taken from distinct samples or whether the same sample was measured repeatedly
☐	☒	The statistical test(s) used AND whether they are one- or two-sided *Only common tests should be described solely by name; describe more complex techniques in the Methods section.*
☒	☐	A description of all covariates tested
☒	☐	A description of any assumptions or corrections, such as tests of normality and adjustment for multiple comparisons
☐	☒	A full description of the statistical parameters including central tendency (e.g. means) or other basic estimates (e.g. regression coefficient) AND variation (e.g. standard deviation) or associated estimates of uncertainty (e.g. confidence intervals)
☐	☒	For null hypothesis testing, the test statistic (e.g. *F*, *t*, *r*) with confidence intervals, effect sizes, degrees of freedom and *P* value noted *Give P values as exact values whenever suitable.*
☒	☐	For Bayesian analysis, information on the choice of priors and Markov chain Monte Carlo settings
☒	☐	For hierarchical and complex designs, identification of the appropriate level for tests and full reporting of outcomes
☒	☐	Estimates of effect sizes (e.g. Cohen's *d*, Pearson's *r*), indicating how they were calculated

Our web collection on statistics for biologists contains articles on many of the points above.

Software and code

Policy information about availability of computer code

Data collection	Microscopy data was obtained using commercially available Leica LAS AF software or Carl Zeiss LSM software, as indicated. 4. Flow cytometry: BD LSRFortessa. Gel imager: Uvidoc-HD2 gel imager. Colony counter: Automated colony counter from Oxford Optronix Ltd.
Data analysis	Data was analyzed by Leica LAS AF (version 2.7.4.10100) and LAS X (version 3.5.6.21594) software, Carl Zeiss LSM (version 14.0.0.0), ImageJ/ Fiji software (version 1.52p) and further processed in Excel (2016) and Prism (version 8.21). Maxquant version 1.6.3.3 was used to analyze quantitative proteomics data. Data was plotted and analyzed using GraphPad Prism 9.0.1. High content IF was analyzed with CellProfiler 4.1.3.

For manuscripts utilizing custom algorithms or software that are central to the research but not yet described in published literature, software must be made available to editors and reviewers. We strongly encourage code deposition in a community repository (e.g. GitHub). See the Nature Research guidelines for submitting code & software for further information.

Data

Policy information about availability of data

All manuscripts must include a data availability statement. This statement should provide the following information, where applicable:

- Accession codes, unique identifiers, or web links for publicly available datasets
- A list of figures that have associated raw data
- A description of any restrictions on data availability

All DRB/TTchem-seq data used in this study is available under GEO accession: GSE148844. All CPD-seq data is available under GEO accession: GSE149082. The SILAC-based quantitative interaction proteomics data have been deposited to the ProteomeXchange Consortium via the PRIDE partner repository with the dataset identifier PXD025304. Source data underlying Figs. 1-6 and all Supplementary Figs. are provided as a Source Data file with this paper. Any other data are available from the corresponding author upon reasonable request.

Field-specific reporting

Please select the one below that is the best fit for your research. If you are not sure, read the appropriate sections before making your selection.

☒ Life sciences ☐ Behavioural & social sciences ☐ Ecological, evolutionary & environmental sciences

For a reference copy of the document with all sections, see nature.com/documents/nr-reporting-summary-flat.pdf

Life sciences study design

All studies must disclose on these points even when the disclosure is negative.

Sample size	sample sizes are specified in the legend to each figure and were chosen based on prior extensive experience in the applied techniques (Ribeiro-Silva 2018, PMID: 30287812; Ribeiro-Silva 2020 PMID: 32985517; Wienholz 2019 PMID:30715484; Steurer 2018 PMID: 29632207; van Cuijck 2015, PMID: 26151477; Dinant 2013; PMID: 23973375;), which allows us to estimate beforehand how many samples should be analyzed to provide sufficient statistical power to distinguish real differences.
Data exclusions	No samples were excluded
Replication	Experiments were replicated as indicated per experiment in the legends. All replication attempts were successful
Randomization	This is not applicable as our sample groups (cells growing in a dish)were grown under the same conditions and collected randomly when given treatment or not without any bias.
Blinding	Blinding was not needed as data is collected by imaging software which yield unbiased, objective measurements.

Reporting for specific materials, systems and methods

We require information from authors about some types of materials, experimental systems and methods used in many studies. Here, indicate whether each material, system or method listed is relevant to your study. If you are not sure if a list item applies to your research, read the appropriate section before selecting a response.

Materials & experimental systems

n/a	Involved in the study
☐	☒ Antibodies
☐	☒ Eukaryotic cell lines
☒	☐ Palaeontology and archaeology
☐	☒ Animals and other organisms
☒	☐ Human research participants
☒	☐ Clinical data
☒	☐ Dual use research of concern

Methods

n/a	Involved in the study
☒	☐ ChIP-seq
☒	☐ Flow cytometry
☒	☐ MRI-based neuroimaging

Antibodies

Antibodies used

53BP1, Santa Cruz, sc-22760
BrdU, (CldU) Abcam, ab6326
BrdU, (IdU) BD Biosciences, B44, 347580
CSA/ERCC8, Santa Cruz, sc376981
CSB/ERCC6, Santa Cruz, sc10459
CSB/ERCC6, Antibodies-online, ABIN2855858
FANCD2, Rb Novusbio, NB100-182
GFP, Roche, 14314500
GFP, Abcam, Ab290
HA, Roche, 11867423001
Lamin B1, Abcam, Rabbit, Cat. num: ab16048, Lot num: GR3244890-2
p62/GTF2H1, Sigma Aldrich, WH0002965M1
RPB1 (Pol II), Cell signalling, D8L4Y
RPB3, Abcam, ab138436
RPB9, Abcam, ab192407
P-Ser2-RPB1, Chromotek, 3E10
SPT4/SUPT4H1, Cell signalling, D3P2W
SPT5/SUPT5H, Bethyl, A300-869A
SSRP1, Biolegend, 609701
Tubulin, Sigma Aldrich, B512
XPD ,Abcam, ab54676

XPF, Santa Cruz, sc-136153
Anti-mouse Alexa 488 , Invitrogen, A11001
Anti-rat Cy3, Jackson Immuno Research, cat# 712-166-153
Anti-Rabbit Alexa 594, Invitrogen, A21207
Anti-Rabbit IRDye 770, Sigma, sab4600215
Anti-Rabbit IRDye 680, Sigma, sab4600200
Anti-Mouse IRDye 680, Sigma, sab4600199
Anti-Mouse IRDye 770, Sigma, sab4600214
Anti-Goat IRDye 770, Sigma, sab4600375
Anti-Rat IRDye 770, Sigma, sab4600479
Details of concentrations used for western blot/immunofluorescence can be found in the antibody information in the Extended Table.

Validation

Antibodies were validated as indicated on their manufacturer's website, where validated in previous publications of our lab by siRNA/KO experiments or where checked by western blot or immunofluorescence in this manuscript, mostly with a siRNA/KO as control for specificity. All the antibodies used in the manuscript showed bands of expected size.
53BP1, Santa Cruz, sc-22760, verified in our lab PMID: 19797077
BrdU, (CldU) Abcam, ab6326, verified in our department PMID: 31337767
BrdU, (IdU) BD Biosciences, B44, 347580, verified in our department PMID: 31337767
CSA/ERCC8, Santa Cruz, sc376981, verified in our department PMID: 29531219
CSB/ERCC6, Santa Cruz, sc10459, verified by siRNA and immunoblotting Extended data fig. 3e
CSB/ERCC6, Antibodies-online, ABIN2855858, Santa Cruz, sc376981, verified in our department PMID: 29531219
GFP, Roche, 14314500, verified by direct comparison by immunoblotting Extended data fig. 2g
HA, Roche, 11867423001, verified by direct comparison by immunoblotting Extended data fig. 2a.
Lamin B1, Abcam, Rabbit, Cat. num: ab16048, Lot num: GR3244890-2
p62/GTF2H1, Sigma Aldrich, WH0002965M1, verified in our department PMID: 32985517
RPB1 (Pol II), Cell signalling, D8L4Y, verified in our lab PMID: 29632207
RPB3, Abcam, ab138436, confirmed by band at correct height that co-IPs with Pol II, fig.2c
RPB9, Abcam, ab192407 confirmed by band at correct height that co-IPs with Pol II, extended data fig.6d
P-Ser2-RPB1, Chromotek, 3E10, D8L4Y, verified in our lab PMID: 29632207
SPT4/SUPT4H1, Cell signalling, D3P2W, verified by siRNA and immunoblotting Extended data fig. 3e
SPT5/SUPT5H, Bethyl, A300-869A, , verified by siRNA and immunoblotting Extended data fig. 3e
SSRP1, Biolegend, 609701, verified in our lab PMID: 23973375
Tubulin, Sigma Aldrich, B512, commonly used a loading control in the lab, verified by specific and intense band at correct height
XPD ,Abcam, ab54676, , verified in our department PMID: 32985517
XPF, Santa Cruz, sc-136153, verified by siRNA and immunoblotting Extended data fig1.i

Eukaryotic cell lines

Policy information about cell lines

Cell line source(s)

HCT116 from Horizon Discovery
MRC-5 sv40 immortalized human lung fibroblast were generated in the lab
C5RO fibroblasts (hTert), CS3BE (CS-A, SV40), XP186LV (XP-C), CS1SP (CS-A, primary) cells were routinely used wt and repair deficient cell types present in the host institute as described in, respectively, PMID: 19797077, PMID: 30715484, PMID: 28088761, PMID: 9381559

Authentication

None were authenticated.

Mycoplasma contamination

All cell lines were routinely tested for mycoplasma and were all negative.

Commonly misidentified lines
(See ICLAC register)

No commonly misidentified cell lines were used in the study.

Animals and other organisms

Policy information about studies involving animals; ARRIVE guidelines recommended for reporting animal research

Laboratory animals

C. elegans strains wild type Bristol N2, GJ1519 csb-1(ok2335), GJ1553 xpc-1(tm3886), HAL505 elof-1(emc203)

Wild animals

This study did not involve wild animals.

Field-collected samples

This study did not involve samples collected from the fields.

Ethics oversight

No ethics oversight is required for studies using C.elegans.

Note that full information on the approval of the study protocol must also be provided in the manuscript.